Imprinted *Dlk1* dosage as a size determinant of the mammalian pituitary gland

Valeria Scagliotti[1], Maria Lillina Vignola[1*], Thea Willis[1*, 2], Mark Howard[3], Eugenia Marinelli[1], Carles Gaston-Massuet[4], Cynthia Andoniadou[2], Marika Charalambous[1#].

[1]Department of Medical and Molecular Genetics, Faculty of Life Sciences and Medicine, King's College London, London SE16RT, UK.

[2]Centre for Craniofacial and Regenerative Biology, Faculty of Dentistry, Oral and Craniofacial Sciences, King's College London, London SE11UL, UK.

[3]MRC Centre for Transplantation, Peter Gorer Department of Immunobiology, School of Immunology & Microbial Sciences, King's College London

[4]Centre for Endocrinology, William Harvey Research Institute, Barts and the London School of Medicine and Dentistry, Queen Mary University of London, London, United Kingdom.

* These authors contributed equally to the work.

Corresponding author.

Abstract

Co-regulated genes of the Imprinted Gene Network are involved in the control of growth and body size, and imprinted gene dysfunction underlies human paediatric disorders involving the endocrine system. Imprinted genes are highly expressed in the pituitary gland, among them, *Dlk1*, a paternally expressed gene whose membrane-bound and secreted protein products can regulate proliferation and differentiation of multiple stem cell populations. Dosage of circulating DLK1 has been previously implicated in the control of growth through unknown molecular mechanisms. Here we generate a series of mouse genetic models to modify levels of *Dlk1* expression in the pituitary gland and demonstrate that the dosage of DLK1 modulates the process of stem cell commitment with lifelong impact on pituitary gland size. We establish that stem cells are a critical source of DLK1, where embryonic disruption alters proliferation in the anterior pituitary, leading to long-lasting consequences on growth hormone secretion later in life.

Introduction

How organ size is determined and maintained throughout life is a key question in biology. This process is complex and depends on the balance of proliferation/differentiation and apoptosis during development, during which the eventual size is attained. Following this, stem cells must repopulate the differentiated cells to maintain a stereotypical number. In some cases organ size and cell composition can change dependent upon the life-cycle stage of the organism, or in response to the environment.

The mammalian anterior pituitary gland (AP) is a master endocrine organ that integrates hypothalamic and peripheral cues to drive the release of circulating hormones. Life events such as stress, puberty and pregnancy-lactation cause remodelling of the AP to allow appropriate levels of hormone production, and changes in cell number and gland size (Perez-Castro et al. 2012). Since the stem cell capacity of SRY-related HMG-box 2 expressing (SOX2+) tissue-resident pituitary stem cells (PSCs) was demonstrated (Andoniadou et al. 2013; Rizzoti, Akiyama, and Lovell-Badge 2013), many teams have integrated knowledge of developmental signalling pathways with information about their determination and maintenance (reviewed (Russell, Lodge, and Andoniadou 2018)). Importantly, the SOX2+ compartment acts not only as a source of cellular progenitors, but also in postnatal life directs the expansion of more committed cells by the production of paracrine signals, including WNT ligands (Russell et al. 2021). Due to these recent advances, the AP is an excellent system in which to study the fundamental process of organ size determination and homeostasis.

Imprinted genes are key determinants of body size in mammals, acting during early life to modulate growth and differentiation pathways (reviewed in (Tucci et al. 2019)). They represent ~100 transcripts in mammalian species that are epigenetically regulated such that only a single parental copy is expressed and the other silenced by a mechanism utilising DNA methylation. Imprinted gene functions converge on a small number of biological processes – neurobiology, placentation and growth (reviewed in (Tucci et al. 2019)). We and others have shown that maintaining imprinted gene expression dosage within a narrow range is key to attaining the balance of growth to organ maturation ((Charalambous et al. 2012; Plagge et al. 2004; Tsai et al. 2002)). We recently noted that imprinted gene expression is enriched in the developing and postnatal pituitary gland, and we proposed that mis-regulation of gene dosage may underlie many of the endocrine features of human imprinting disorders including Silver Russell and Prader Willi Syndromes (Scagliotti et al. 2021). Importantly, a previously identified co-regulated subset of these genes, known as the imprinted gene network (IGN, (Varrault et al. 2006)), are co-expressed and represent some of the most abundant transcripts in the developing pituitary gland (Scagliotti et al. 2021).

Delta-like homologue 1 (*Dlk1*), a paternally-expressed imprinted gene on mouse chromosome 12 (Schmidt et al. 2000; Takada et al. 2000), is a member of the IGN. The syntenic area on human chromosome 14 is the critical region for Temple Syndrome, and loss of *DLK1* expression is thought to cause phenotypes associated with this disorder; pre-and postnatal growth restriction with increased truncal obesity and precocious puberty (Ioannides et al. 2014). Alternative splicing of *Dlk1* results in several protein variants that have important functional differences. Full-length *Dlk1* encodes a ~60kD protein that may be cleaved by the TACE protease ADAM17 at the extracellular cell surface to release

soluble DLK1 into the circulation. Alternative splicing events skip the ADAM17 recognition site, resulting in a transmembrane form of DLK1 which cannot be cleaved (Smas, Chen, and Sul 1997). The signalling pathway by which DLK1 acts has yet to be elucidated**.** *Dlk1* encodes a protein with high sequence similarity to the NOTCH ligand Delta, but it lacks the DSL domain critically required for NOTCH interaction (Smas and Sul 1993).

DLK1 is expressed in several progenitor cell populations where its expression is associated with the self-renewal to differentiation transition (reviewed in (Sul 2009)). For example, addition of soluble DLK1 to cultured preadipocytes results in failure of these cells to differentiate into adipocytes whereas deletion of this gene causes premature differentiation (Smas and Sul 1993). In the context of the postnatal neurogenic niche, the expression dosage of both membrane-bound and secreted DLK1 regulates the rate of self-renewal of the SOX2+ neural stem cells (Ferron et al. 2011).

In mice, *Dlk1* expression is first detected from mid-gestation in a variety of mesodermal and neuroendocrine cell types, including the developing pituitary gland (da Rocha et al. 2007). After birth *Dlk1* expression is rapidly reduced, serum levels fall, and expression becomes restricted to a limited number of cell types including some neurons, adrenal and AP cells (Sul 2009). In adult humans *DLK1* is expressed in Growth Hormone (GH)-producing somatotrophs (Larsen et al. 1996). We and others have shown that *Dlk1* knockout mice are small with reduced GH production ((Puertas-Avendano et al. 2011; Cheung et al. 2013; Cleaton et al. 2016)). However, *Gh* mRNA is not reduced following a conditional ablation of *Dlk1* in mature somatotrophs (Appelbe et al. 2013). We previously demonstrated that serum GH levels are elevated in mice that overexpress *Dlk1* from endogenous control elements at 6 months of age, and that their GH levels fall less markedly following high-fat diet feeding (Charalambous et al. 2014). In contrast, pregnant dams lacking circulating DLK1 in pregnancy have a blunted increase in pregnancy-associated GH production (Cleaton et al. 2016). These data led us to hypothesise that DLK1 dosage modulates the size of the GH reserve at critical life stages, and prompted us to investigate the molecular mechanism further.

Here we manipulate *Dlk1* gene dosage in mice using both knock out and overexpression models. We show that *Dlk1* dosage regulates AP size independently of whole body weight, suggesting an autocrine/paracrine role for the product of this gene. Loss of *Dlk1* function leads to reduced AP volume by acting in a discrete developmental window to shift the balance of stem cell replication/commitment, by mediating the sensitivity of progenitor cells to the WNT pathway. Finally, increased *Dlk1* expression dosage increases the SOX2+ stem cell compartment, influencing organ expansion throughout the life course and increases the rate of postnatal replication in committed cells. This indicates that DLK1 may

act postnatally to mediate paracrine signals between the stem and committed cell compartment of the AP. Overall we conclude that *Dlk1* dosage determines pituitary size and postnatal stem cell homeostasis.

Results

Increasing the expression dosage of Dlk1 causes pituitary hyperplasia without tumorigenesis.

We previously demonstrated that adult GH was elevated in a transgenic model where extra copies of the *Dlk1* gene are introduced in the context of a 70kb bacterial artificial chromosome (BAC, $TG^{Dlk1\text{-}70C}$) (Charalambous et al. 2014). This transgene drives gene expression in a similar temporal and tissue-specific pattern to the endogenous gene, but imprinting is not maintained due to lack of inclusion of the imprinting control region for the chromosome 12 cluster ((da Rocha et al. 2009), Figure 1A). In the pituitary gland at 12 weeks of age, $TG^{Dlk1\text{-}70C}$ hemizygous mice (hereafter WT-TG) had increased *Dlk1* mRNA expression 2-3 fold compared to wild-type (WT, Figure 1B). This resulted in elevated protein expression of all of the major isoforms of DLK1 (Figure 1C). In the adult AP, DLK1 was expressed in a subpopulation of all hormone-producing cells except corticotrophs (Figure 1D). The transgenic model did not modify the proportion of cells in the population that were DLK1+ (WT 36.5±0.9%; WT-TG 36.3±0.8%), rather, the same fraction of cells produced more protein (Figure 1C). Immunohistochemical staining for DLK1 clearly indicated that a proportion of the protein is membrane-localised (Figure 1D).

To investigate the physiological basis of increased GH production we conducted a stereological analysis of the AP at 12 weeks in WT-TG mice and their WT littermates. Pituitary size was increased following *Dlk1* overexpression (Figure 1E, F), but the proportions of hormone-producing cells were not affected (Figure 1D and Supplementary Table 1). Cell size was unaffected by genotype (not shown), and we saw no evidence of pituitary tumours in any animal examined up to 1 year of age. Overall, this resulted in a 38% expansion in the somatotroph population, potentially increasing the GH-secretory reserve in WT-TG animals (Figure 1G). Thus, increasing the expression dosage of *Dlk1* causes pituitary hyperplasia without a shift in hormone-producing cell fate. These data suggested that *Dlk1* might be acting during pituitary development to modulate AP size.

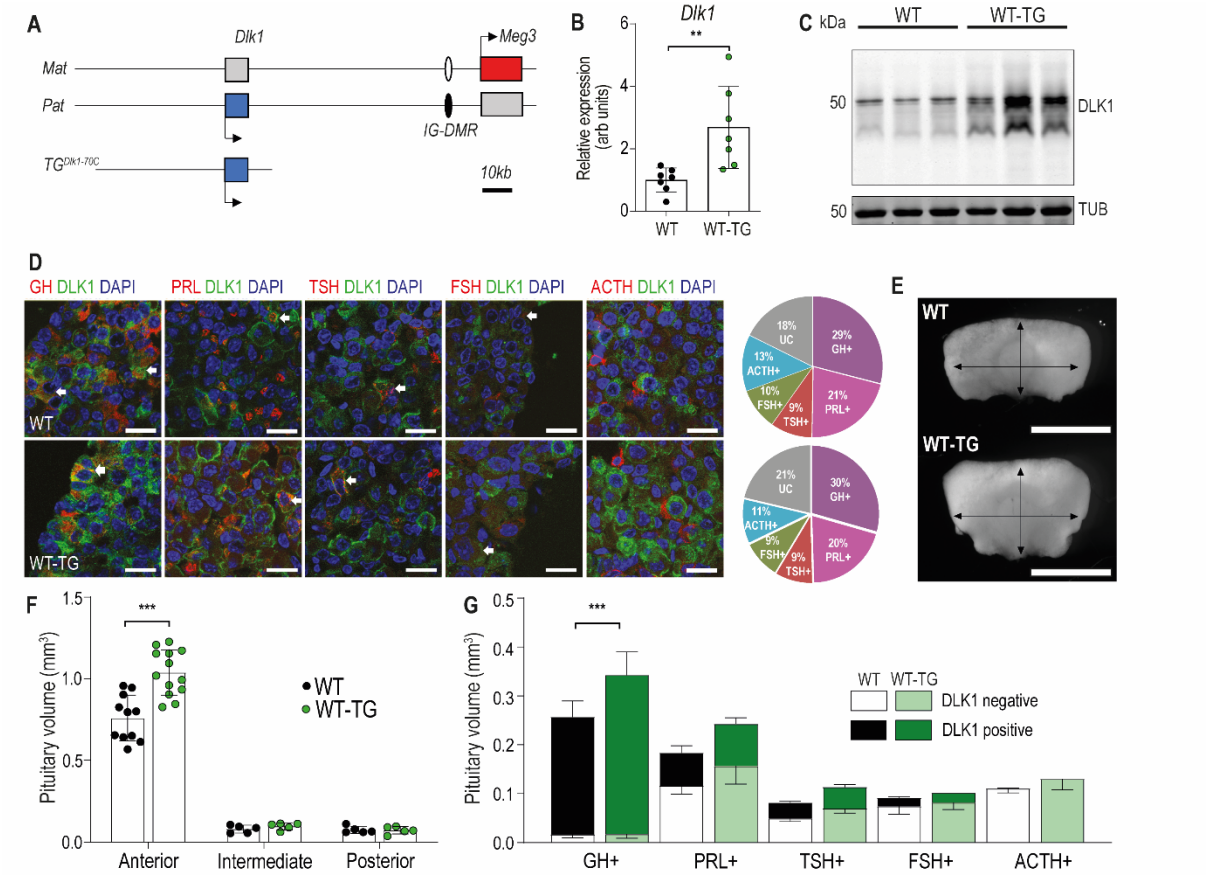

Figure 1. Increasing the expression dosage of *Dlk1* causes pituitary hyperplasia. (A) Schematic of part of the imprinted region on mouse chromosome 12 that contains the *Dlk1* and *Meg3* genes. *Dlk1* is expressed (blue box) from the paternally-inherited chromosome, *Meg3* from the maternally-inherited chromosome (red box). This expression pattern is established and maintained by an intergenic differentially methylated region (IG-DMR) which is paternally methylated (black oval) and maternally unmethylated (white oval). The $TG^{Dlk1\text{-}70C}$ transgene used in this study contains the whole *Dlk1* gene within ~70kb of surrounding DNA, but does not contain the IG-DMR and is not imprinted. (B) RT-qPCR for *Dlk1* in whole pituitary from 12-week old female hemizygous $TG^{Dlk1\text{-}70C}$ transgenic (WT-TG) mice and wild-type (WT) littermates. *Dlk1* expression is 2.7x higher in transgenic animals, **p < 0.01 compared by Mann-Whitney U test, n = 7 per genotype. Bar shows mean +/- SD. (C) Western blots of extracts from whole pituitary of 12wk female WT and WT-TG mice. Alpha tubulin (TUB) is used as a loading control. Full-length and membrane bound isoforms at 50-60kDa. (D) Fluorescence immunohistochemistry for DLK1 and pituitary hormones at 12wk. DLK1 in the adult AP is detected in all hormone-producing cells except corticotrophs; GH = somatotrophs, PRL = lactotrophs, TSH = thyrotrophs, FSH = gonadotrophs; ACTH = corticotrophs. Scale bar = 20um. Note some membrane localisation of DLK1. White arrows indicate co-expression. Proportion of hormone-labelled cells was quantified between mice of each genotype and shown as a pie chart on the right, UC = unclassified cell type. (E) Whole pituitary glands from adult WT-TG mice appear larger than those from WT littermates. Light field image of 12wk female glands, scale bar = 1mm. (F) Anterior pituitary volume, but not intermediate lobe or posterior pituitary volume is increased in WT-TG animals compared to WT littermates. 12-week old females, n = 12/13 animals per genotype, compared by 2-Way ANOVA with Sidak's post-hoc multiple comparison test, *** p<0.001. (G) Overall cell proportion was not changed but absolute volume of hormone-producing cells was altered by *Dlk1* dosage. Data from Table S1 normalised for pituitary volume, groups are compared by 2-Way ANOVA and differ significantly

according to genotype (p = 0.004); genotypes are compared for each cell type Sidak's multiple comparison test – WT and WT-TG animals have a significantly different proportion of GH-producing cells (*** p < 0.001). F and G bars show mean values +/- SD.

Modulation of DLK1 gene dosage in the developing pituitary gland.

In order to understand how *Dlk1* regulates pituitary size we generated embryos where the gene expression is increased (WT-TG), ablated (deletion of *Dlk1* from the active paternal allele, PAT) or ablated but expressing the transgene (PAT-TG) from matched litters (Figure 2A). In the whole pituitary gland at E18.5 *Dlk1* splice forms expressed from the $TG^{Dlk1\text{-}70C}$ transgene appeared similar in type and abundance to those expressed from the endogenous locus (Figure 2B, C).

Dlk1 is expressed from early development of the AP, from at least E9.5 in Rathke's pouch (RP) and the overlying ventral diencephalon (Figure 2D). As development proceeds, *Dlk1* levels remain high both in progenitor cells of the cleft and lineage committing cells of the parenchyma (Figure 2D, WT and WT-TG). *Dlk1* expression could not be detected in PAT embryos at any stage, confirming that genomic imprinting is maintained in this tissue. Surprisingly, when expression from the $TG^{Dlk1\text{-}70C}$ transgene was examined in the absence of the endogenous allele, we could not detect *Dlk1* in the early development of the AP or midbrain. Rather, *Dlk1* expression was first detected in parenchymal cells at E15.5 of PAT-TG animals. In contrast, other tissues such as cartilage demonstrated robust expression of *Dlk1* in a pattern similar to that of the endogenous gene (Figure 2D). DLK1 protein expression mirrored that of the mRNA at E18.5 (Figure 2E) and at postnatal day 21 (P21) a similar pattern was observed. These data indicate that endogenous *Dlk1* is expressed from the onset of pituitary development, in both progenitor and lineage committing cells, and that some regulatory sequences necessary for the full repertoire of *Dlk1* gene expression are not located within the 70kb genomic region delineated by the transgene.

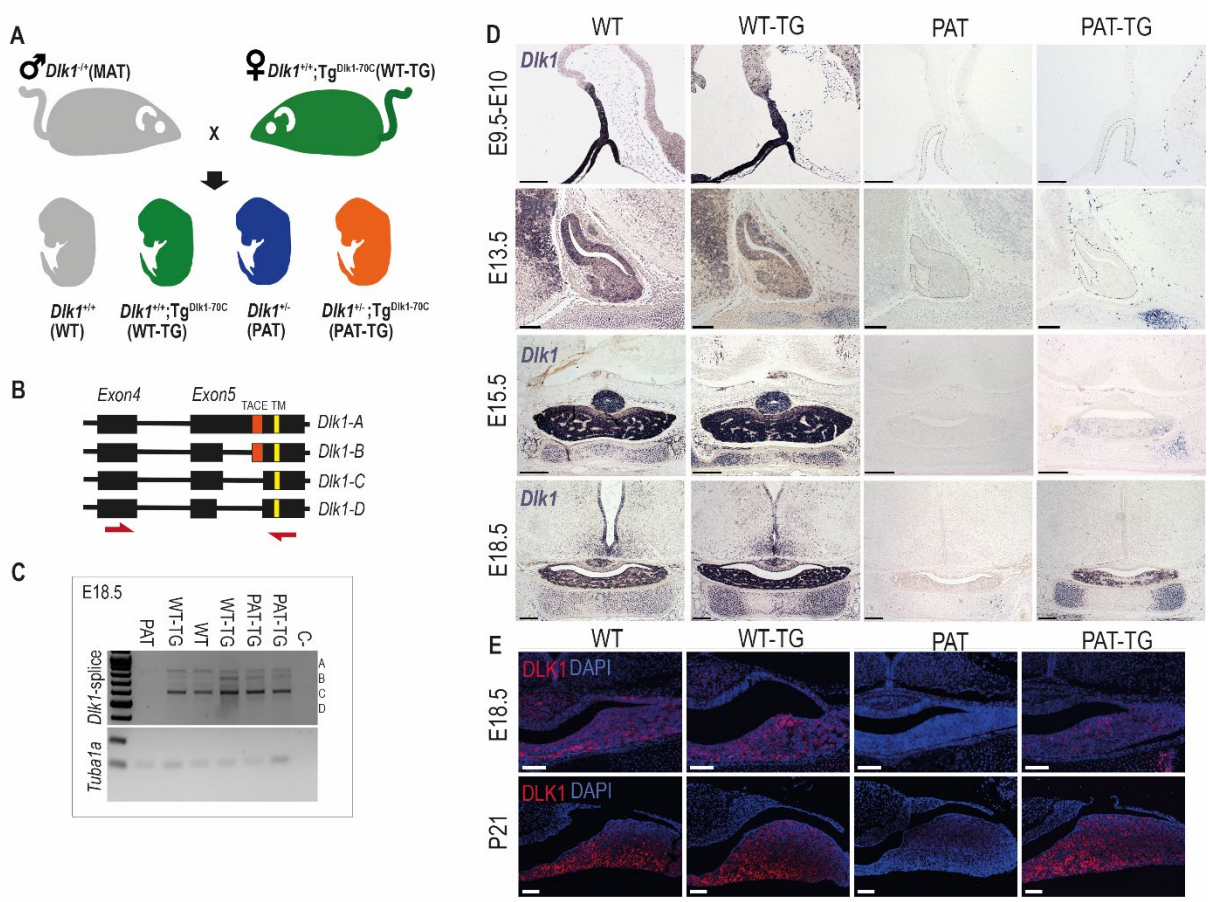

Figure 2. *Dlk1* imprinting and expression in the developing pituitary gland from the endogenous locus and *TG*$^{Dlk1\text{-}70C}$ transgene. (A) Cross used to generate embryos and postnatal animals in the study. Males inheriting the deleted allele from the mother (maternal *Dlk1*$^{tm1Srbpa/+}$ heterozygotes or MATs) were crossed to females hemizygous for the *TG*$^{Dlk1\text{-}70C}$ transgene (WT-TG), generating 4 genotypes, WT, WT-TG, paternal *Dlk1* $^{+/tm1Srbpa}$ heterozygotes (PATs) and mice inheriting a deleted paternal allele and the transgene (PAT-TG). (B) Schematic showing the known splice variants of *Dlk1*, A-D. Splicing occurs internally in exon 5 of the *Dlk1* gene. *Dlk1*-A and B retain an extracellular cleavage domain (TACE), in Dlk1-C and D this region is spliced out. All versions contain a single pass transmembrane domain (TM). Red arrows indicate location of primers used in (C). (C) Semi-quantitative PCR on embryonic day (E)18.5 whole pituitary glands from the 4 genotypes shown in (A). Top – primers amplify the exon 4-5 region of *Dlk1* and can distinguish splice variants based on size. Bottom – alpha-tubulin (*Tuba1a*) was amplified as a loading control on each sample. (D) *In-situ* hybridisation for *Dlk1* in the developing pituitary gland from E9.5 to E18.5 in the 4 genotypes shown in (A). *Dlk1* expression is indicated by purple staining. Scale bars show 100um (E9.5 and E13.5, sagittal sections) and 200um (E15.5 and E18.5, frontal sections). (E) Immunohistochemistry (IHC) for DLK1 on frontal sections at E18.5 and postnatal day 21 (P21), counterstained with DAPI. Scale bars = 50um.

Dlk1 exhibits complex temporal and spatial regulation in the AP which is only partially recapitulated by the TG$^{Dlk1\text{-}70C}$ *transgene.*

Since DLK1 expression in the pituitary progenitor/stem population has not previously been described in detail, we examined its temporal co-expression with the stem cell marker SOX2. In late embryogenesis

and postnatally SOX2+ PSCs occupy the periluminal marginal zone (MZ) of the pituitary gland. In WT and WT-TG E18.5 embryos, DLK1 is clearly co-expressed with SOX2 in this compartment (Figure 3A). However, by postnatal day 21 (P21), DLK1+ cells are largely absent from the MZ of animals with an intact *Dlk1* gene (Figure 3B). As expected, deletion of *Dlk1* from the paternal allele ablates all protein expression. However, expression from the $TG^{Dlk1\text{-}70C}$ transgene was absent from the MZ at both stages.

We recently reanalysed publicly-available single-cell sequencing (scRNA-seq) data of the mouse pituitary gland generated by the Camper lab (Cheung et al. 2018), (Cheung and Camper 2020) in order to catalogue imprinted gene expression in the early postnatal (P4) and adult (P49) gland (Scagliotti, 2021). These data confirmed our immunohistochemical analyses (Figure 1D) of enriched expression of *Dlk1* in somatotrophs, lactotrophs and thyrotrophs, as well as in a subset of *Sox2*-expressing stem cells (Figure 3C). The scRNA-seq data also appeared to confirm the reduction in *Dlk1* gene expression in the stem cell compartment between early and late postnatal stages (17.6% at P4 to 14.8% at P49, Figure 3C). Similarly, the proportion of cells expressing *DLK1* in the human postnatal PSC compartment decreases from youth to adulthood as shown by analyses on human snRNA-seq pituitary datasets (Zhang et al. 2022) (14.1% in infant, 5.7% in adult and 8.9% in aged, Figure 3D). As in the mouse, *DLK1* expression in the human pituitary is most abundant in somatotrophs, lactotrophs and thyrotrophs. These three cell types are derived from a common embryonic lineage progenitor expressing the transcription factor POU1F1, and the mature hormonal lineages continue to express this transcription factor to directly regulate hormonal genes (Camper et al. 1990; Li et al. 1990). We found a high level of co-expression between DLK1 and POU1F1 in the WT and WT-TG pituitary gland at E18.5, though DLK1+ cells were also clearly visible in the MZ and in POU1F1- parenchymal cells (Figure 3E). In contrast, in the PAT-TG pituitary, DLK1 expression was confined solely to POU1F1+ cells. These data indicate that the $TG^{Dlk1\text{-}70C}$ transgene contains *cis* regulatory sequences necessary for *Dlk1* expression in POU1F1+ cells but not those required for expression in stem cells and other hormonal lineages (Figure 3F). To determine whether *Dlk1* might be a direct target of POU1F1 we explored a POU1F1 ChIP-seq dataset from GH-expressing cells derived from rats (Skowronska-Krawczyk et al. 2014). By mapping the rat POU1F1 binding sites onto the mouse genome we identified 3 potential POU1F1 binding sites within 120kb of the *Dlk1* gene (Figure S1). These sites overlapped other genomic features indicative of regulatory activity including evolutionary conservation, CpG islands and previously mapped histone modifications associated with enhancer activity in the embryonic brain (Gorkin et al. 2020). One of these binding sites was localised within the 70kb included in the $TG^{Dlk1\text{-}70C}$ transgene. We suggest that *Dlk1* is likely to be a direct POU1F1 target in both the WT and $TG^{Dlk1\text{-}70C}$ transgenic mice.

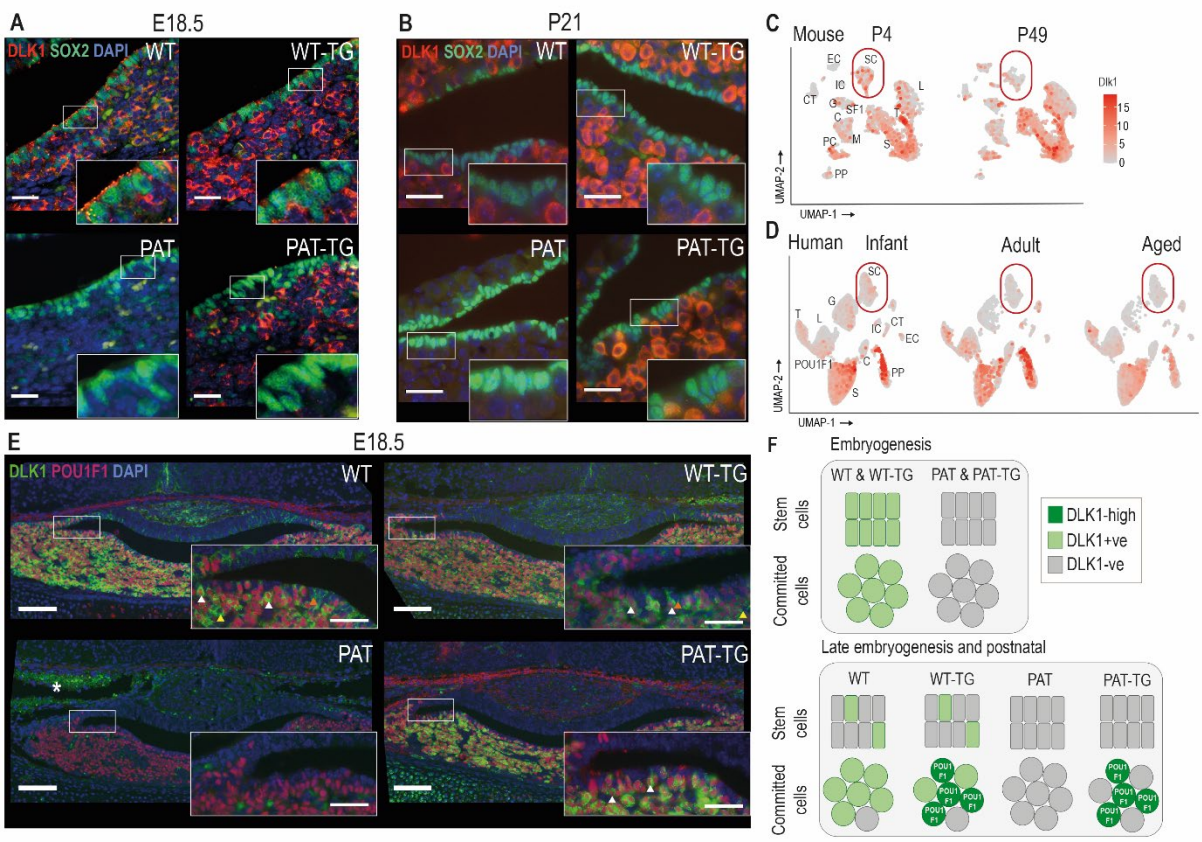

Figure 3. DLK1 expression in the pituitary gland is dynamically regulated in two distinct compartments, only one of which is recapitulated by the *TG*$^{Dlk1\text{-}70C}$ transgene. (A) IF of DLK1 and SOX2 in the E18.5 pituitary. SOX2 expression is high in the epithelial cells lining the pituitary lumen, as expected. In WT and WT-TG mice there is co-expression of DLK1 and SOX2 (inset), as well as high levels of DLK1 expression in the SOX2-negative parenchyma. In the PAT-TG pituitary DLK1 expression is not detected in the SOX2-positive compartment. Scale bars = 25um. (B) IF of DLK1 and SOX2 in the P21 pituitary. The majority of DLK1 expression is outside the SOX2-positive compartment of all genotypes. Scale bars = 25um. (C) UMAP plot illustrating expression of *Dlk1* in sc-RNAseq at P4 (Cheung and Camper 2020) and P49 mice (Cheung et al. 2018) in the postnatal mouse pituitary, indicating high expression in the POU1F1 lineage (S somatotrophs, T thyrotrophes, L lactotrophs), with additional expression in a subset of *Sox2*-positive stem cells (SC), outlined by red box. EC endothelial cells, IC immune cells, CT connective tissue, G gonadotrophs, SF1 steroidal factor 1 progenitors, C corticotrophs, M melanotrophs, PC proliferating cells, PP posterior pituitary. (D) UMAP plot illustrating expression of *DLK1* in sn-RNAseq from infant, adult and aged human pituitary gland (Zhang et al. 2022), indicating high expression in the POU1F1 lineage (S somatotrophs, T thyrotrophs, L lactotrophs), with additional expression in a subset of *SOX2*-positive stem cells (SC). Additional cell labels as in (C). (E) IF of DLK1 and POU1F in the E18.5 pituitary. DLK1 and POU1F1 are highly co-expressed in all *Dlk1*-expressing genotypes (white arrows). In WT and WT-TG there is additional DLK1 expression in marginal zone cells (orange arrow) and parenchymal cells (yellow arrow) that are POU1F1-negative. This expression is absent from the PAT-TG. Scale bar = 100um, inset 25um. * indicates background autofluorescence from blood cells. (F) Summary of *Dlk1* expression across embryonic and early postnatal development in the mouse, with contribution from the transgene.

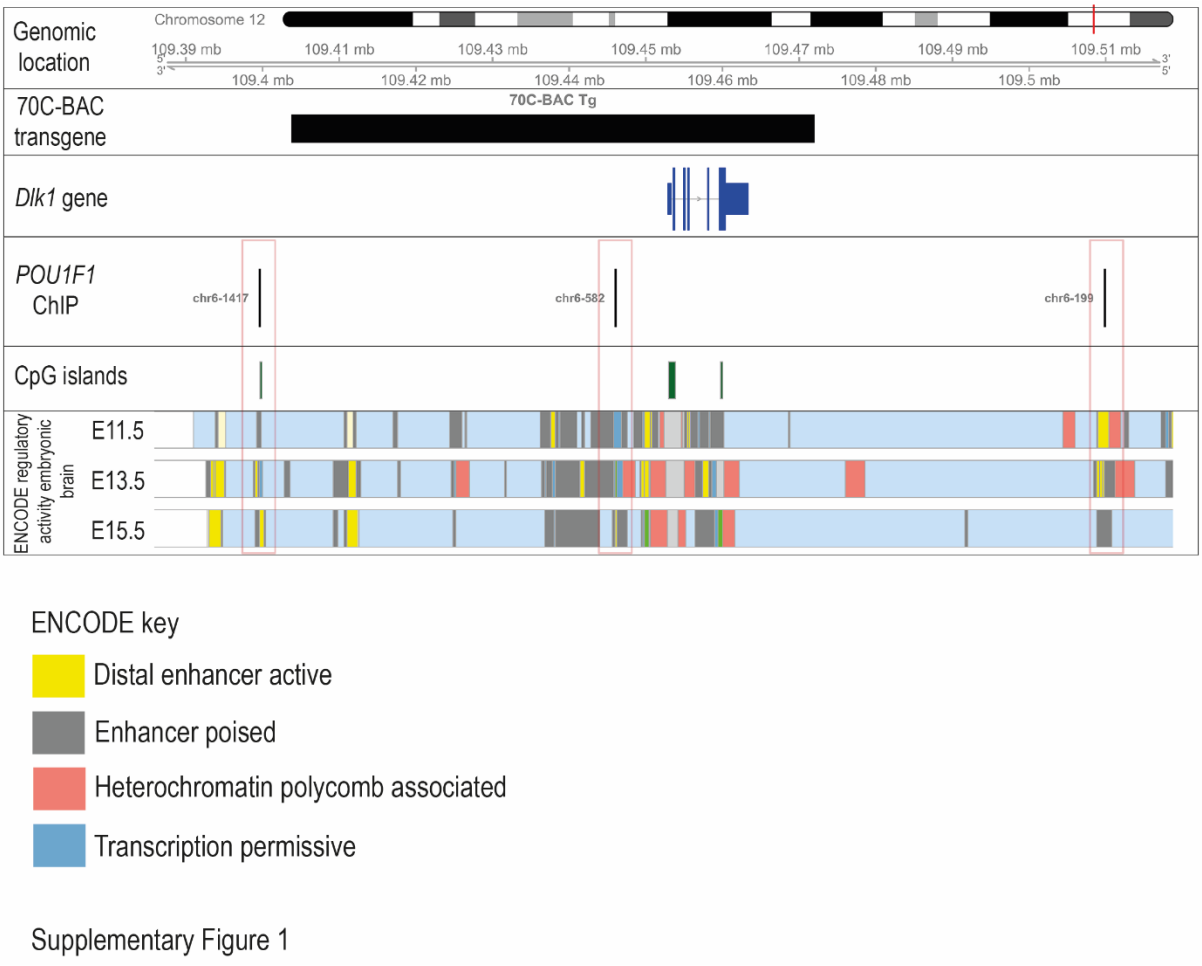

Supplementary Figure 1

Figure S1 (related to Figure 3) *Dlk1* may be a direct transcriptional POU1F1 target. Schematic showing relative genomic positions of sequences in the *TG*$^{Dlk1\text{-}70C}$ transgene and experimentally-verified binding sites for POU1F1 (Skowronska-Krawczyk et al. 2014). 3 predicted POU1F1 binding sites are within 120kb of the *Dlk1* promoter, each within highly conserved regions of the genome and overlapping genomic sites enriched for enhancer-specific histone marks in embryonic forebrain (Gorkin et al. 2020). Only one POU1F1 binding site is predicted to be present in the transgene, mapping ~10kb upstream of the *Dlk1* promoter.

Dlk1 dosage modulation controls AP volume in two distinct developmental periods and independently of body size.

We next explored the consequences of *Dlk1* dosage modulation on pituitary size by performing stereological volume measurements on a time course of embryonic and postnatal pituitaries. First addressing whole organism weight, we determined that PAT animals were growth restricted (~85% WT weight at E18.5) in late gestation, as previously reported (Cleaton et al. 2016). WT-TG mice were not significantly altered in mass, but the $TG^{Dlk1\text{-}70C}$ transgene rescued some of the growth deficit on a *Dlk1*-deleted background; PAT-TG animals weighed ~92% WT mass at E18.5 (Figure 4A, and Table S2). Postnatally PAT animals were further growth restricted, reaching a minimum proportion of WT weight at P14 (~55%), after which the animals commenced catch-up growth, reaching 82% WT weight by weaning at P21. In contrast, the volume of the AP is already significantly reduced in size at E13.5 (61% WT), prior to embryonic growth restriction. As predicted by the lack of *Dlk1* expression from the $TG^{Dlk1\text{-}70C}$ transgene at this stage (Figure 2B), the WT vs WT-TG and PAT vs PAT-TG are indistinguishable in volume (Figure 4B, C, Table S3A, B)). Subsequently, the *Dlk1*-ablated AP maintains this deficit in volume (50-65% WT volume) into postnatal life, with some evidence of volume catch-up at weaning. The $TG^{Dlk1\text{-}70C}$ transgene is unable to consistently rescue the deficit in pituitary volume that is established during embryogenesis (PAT and PAT-TG pituitary volumes are broadly overlapping). In contrast, in WT-TG animals increased *Dlk1* expression from the $TG^{Dlk1\text{-}70C}$ transgene did cause an increase in pituitary volume. This increase in volume was evident in the second postnatal week and became statistically significant at P21 (133% WT volume, consistent with 38% increased AP mass as adults, Figure 3C, 1F). Adjacent structures, the posterior pituitary and postnatal intermediate lobe volume did not differ between genotypes (Table S3A, B) indicating that *Dlk1* acts selectively on pathways that regulate AP size. Moreover, AP hyperplasia only develops when elevated *Dlk1* expression in the parenchyma interacts with a *Dlk1*+ stem cell compartment.

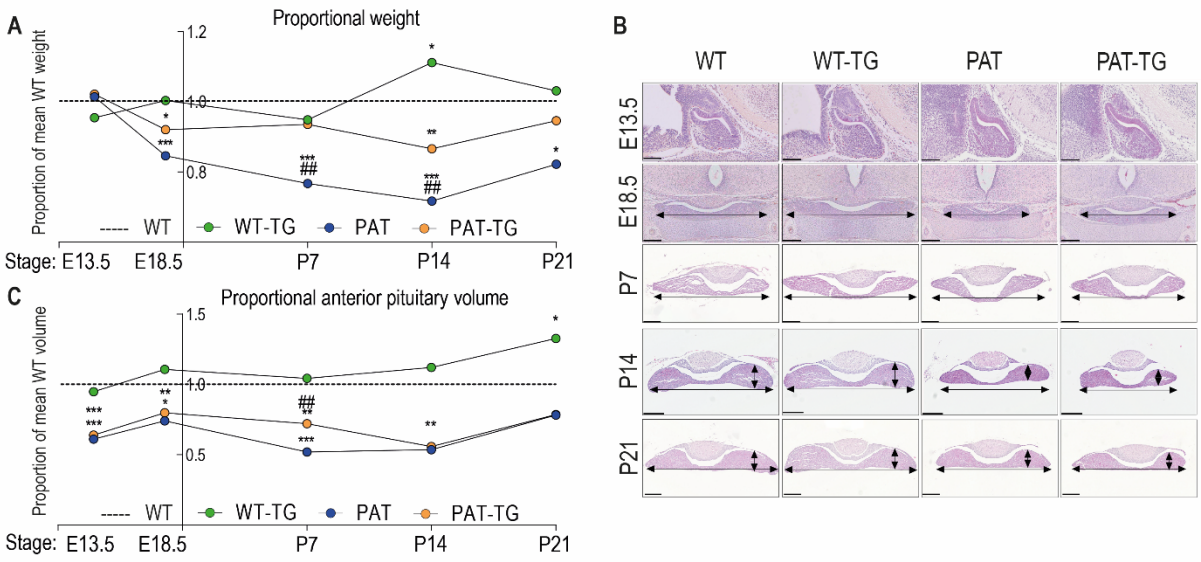

Figure 4. **DLK1 dosage during embryogenesis and early life modulates anterior pituitary volume independent of whole animal mass.** (A) Time-course of proportional body weight by genotype from E13.5 to P21, derived from data in **Table S2**. Lines and points show mean proportional weight of embryo/pup for WT-TG, PAT and PAT-TG animals compared to WT littermates (dotted line at 1.0). The unmodified weight data was compared using a One-Way ANOVA with Bonferroni's posthoc test comparing each genotype with WT (*p<0.05, ***p<0.001), and PAT with PAT-TG (## p<0.01). (B) Haemotoxylin and eosin-stained pituitary glands at E13.5 (sagittal view), E18.5, P7 and P21 (frontal view) across the 4 genotypes. Scale bars show 100um (E13.5), 200um (E18.5, P7) and 300um (P14, P21). (C) Time-course of proportional pituitary volume by genotype from E13.5 to P21, derived from data in **Table S3A, B**. Lines and points show mean volume of the anterior pituitary gland for WT-TG, PAT and PAT-TG animals compared to WT littermates (dotted line at 1.0). Genotypes were compared in unmodified volume data using a One-Way ANOVA with Bonferroni's posthoc test comparing each genotype with WT (*p<0.05, **p<0.01, ***p<0.001), and PAT with PAT-TG (## p<0.01).

Dlk1 dosage modulation does not prevent hormone expression but modifies GH levels and pubertal physiology.

We surveyed the expression of pituitary hormones at E18.5, when all of the hormonal axes have been established. Loss or gain of *Dlk1* dosage did not cause any gross change in hormonal cell localisation or expression at this stage (Figure S2A-Y). To investigate if the increased AP volume in the WT-TG animals has any physiological consequences we measured GH levels in female mice in the peri-pubertal period. In mice, GH levels rise around weaning in the third postnatal week to reach adult levels by the fifth postnatal week (Figure S2Z). GH levels were elevated in young WT-TG mice and though the trend was detected later it became obscured by considerable variability (Figure S2Z). We could not detect a reduction in GH levels in PAT mice at any stage (data not shown). Temple Syndrome and *DLK1* mutations in humans are associated with precocious menarche (Ioannides et al. 2014; Dauber et al. 2017). Using day of vaginal opening (VO) as a proxy for onset of puberty we determined that,

contrary to our expectations, increased expression of *Dlk1* resulted in earlier pubertal onset. However, deletion of *Dlk1* did not alter the timing of puberty, but females were relatively smaller when they entered this state (Figure S2AA).

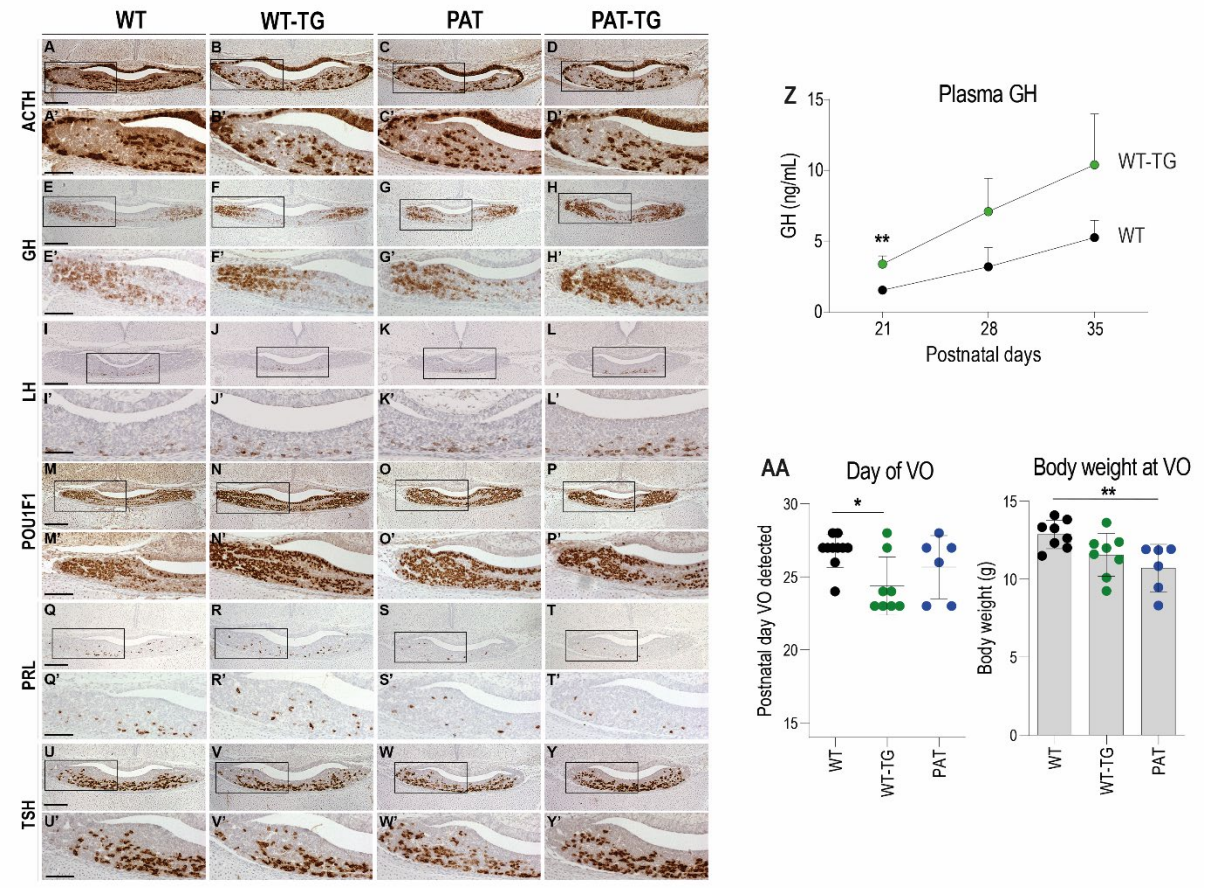

Figure S2 (related to Figure 4). *Dlk1* dosage modulates hormone levels and early life endocrine physiology. (A-Y) Representative images of IHC showing hormone expression at e18.5 of ACTH (A-D, A'-D'), GH (E-H, E'-H'), LH (I-L, I'-L'), POU1F1 (M-P, M'-P'), PRL (Q-T, Q'-T'), TSH (U-Y, U'-Y') with 2-3 animals per genotype examined. Marker expression is stained in brown with haemotoxylin counterstaining in blue. Scale bar = 200um, boxed = 100um. (Z) Circulating GH measured in plasma from WT-TG mice and their WT littermates at postnatal day 21 (P21, n = 9/10), P28 (n = 7/9) and P35 (n = 10/11). Genotypes had significantly different levels of GH (Two-Way ANOVA p = 0.036 by genotype) with Bonferroni post-hoc testing at each time point **p<0.01. (AA) Day of detection of vaginal opening (VO) in female mice (left) and body weight on that day (right) in WT (n=8-10), WT-TG (n = 8) and PAT (n = 6) mice. WT-TG entered puberty by this measure earlier than WT littermates. PAT mice weighed significantly less than WT when VO was detected. Genotypes were compared using a One-way ANOVA with Dunn's multiple comparison test, *p< 0.05, **p<0.01. Bars show mean and SD.

Dlk1 regulates embryonic pituitary size by acting in a discrete developmental window to shift the balance of stem cell replication/commitment.

Dlk1 is expressed from the onset of pituitary morphogenesis in Rathke's pouch and the overlying ventral diencephalon (Figure 2D). Despite this early expression, we could detect no difference in the expression of transcription factors and signalling molecules that have previously been shown to regulate morphogenesis and growth of the gland at this stage (Figure S3). From ~E13.5 , as pituitary progenitor cells exit the cell cycle and differentiate they move dorsally away from the periluminal cleft (Davis, Mortensen, and Camper 2011). Proliferating cells proximal to the lumen of the cleft are SOX2+. DLK1 expression is found in the SOX2+ proliferating cells in the cleft as well as in the newly differentiating cells (Figure 2D). Loss of *Dlk1* in PAT and PAT-TG animals caused a transient reduction in cell proliferation in the cleft at E13.5 (Figure 5A-D, Table S4). There was a concomitant increase in the proportion of cells expressing the lineage marker POU1F1 (Figure 5E, G). Several molecular signalling pathways have been proposed to regulate the emergence of the POU1F1 lineage including NOTCH (Zhu et al. 2006) and WNT pathways (Potok et al. 2008), (Olson et al. 2006). While nuclear HES1, a marker of active NOTCH signalling, was abundantly expressed in the AP at this timepoint, we did not observe a difference in the proportion of HES1+ nuclei between *Dlk1* genotypes (Figure 5F, H). However, we detected increased expression of *Lef1* and *Axin2*, downstream targets of the WNT/β-catenin pathway (Hovanes et al. 2001), (Jho et al. 2002) (Figure 5I). Taken together, we propose that loss of *Dlk1* in PAT and PAT-TG animals reduces AP size by altering the balance of cells remaining in the replicating stem cell pool to those that commit to the *Pou1f1* lineage (Figure 5J). This balance may be shifted by the action of *Dlk1* on the WNT/β-catenin pathway (Figure 5I).

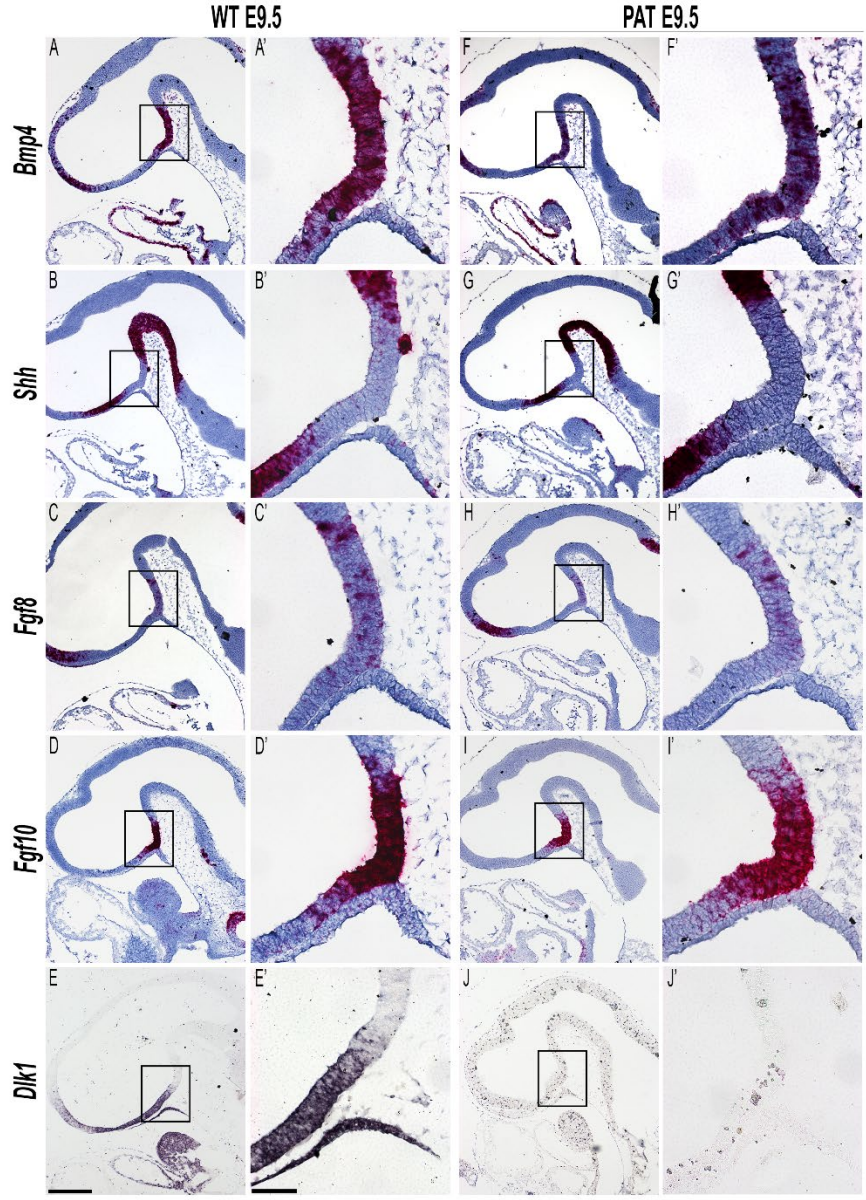

Figure S3 (related to Figure 5). Altered dosage of *Dlk1* does not affect expression of early morphological signalling genes in Rathke's pouch. Representative images of mRNA *in situ* hybridisation in E9.5 wild type (WT) and *Dlk1*-paternal heterozygote (PAT) embryos using specific probes against *Bmp4* (A, A'; F, F'), *Shh* (B, B'; G, G'), *Fgf8* (C, C'; H, H'), *Fgf10* (D, D'; I, I'), all red with blue haemotoxylin counterstaining, and *Dlk1* (E, E'; J, J') purple, no counterstaining. At least 3 animals per genotype were examined. Scale bar = 200um for main images and 50um for boxed images.

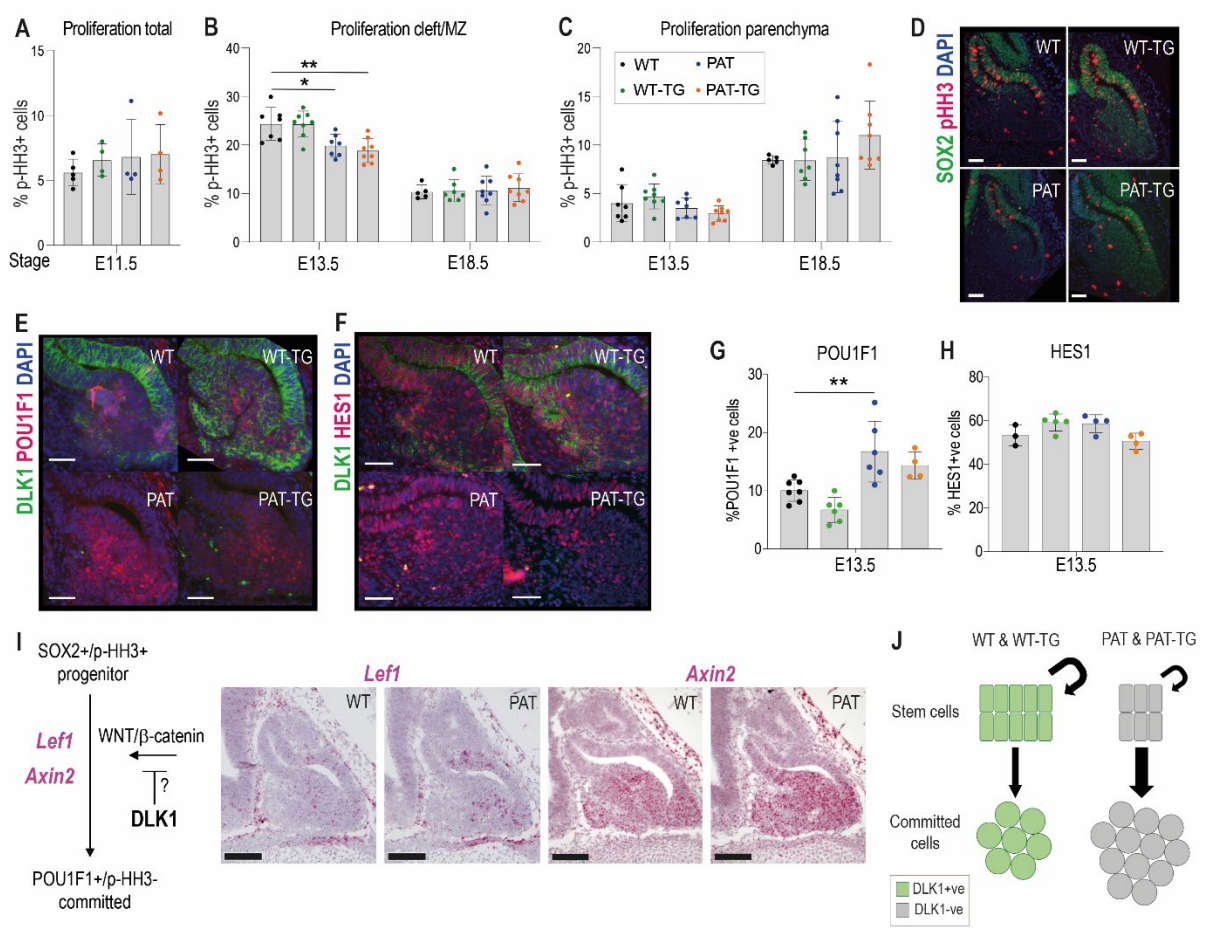

Figure 5. Loss of *Dlk1* expression in an embryonic time window shifts progenitor cells from proliferation to differentiation. (A) Proportion of phospho-histone H3 (pHH3)-positive cells to total cells in the pituitary at E11.5.(B) Proportion of pHH3-positive cells in the morphological stem cell compartment (cleft/marginal zone (MZ)) at E13.5 and E18.5 across the 4 *Dlk1* genotypes. (C) Proportion of pHH3-positive cells in the parenchymal region across the 4 *Dlk1* genotypes. (B) and (C) for each time point genotypes were compared using a One-Way ANOVA with Bonferroni's posthoc test comparing each genotype with WT (*p<0.05, **p<0.01), and PAT with PAT-TG. (D) Representative image showing increased proliferation in the SOX2+ stem cell compartment of *Dlk1*-expressing (WT and WT-TG) embryos at E13.5 compared to non-expressing embryos (PAT and PAT-TG). (E) Representative image showing increased number of POU1F1 cells newly differentiating in the parenchyma of the *Dlk1* non-expressing E13.5 pituitary (PAT and PAT-TG), compared with the *Dlk1*-expressing (WT and WT-TG) gland. (F) Representative image showing no difference in the number of cells expressing nuclear HES1 in *Dlk1*-expressing (WT and WT-TG) embryos at E13.5 compared to non-expressing embryos (PAT and PAT-TG). D-F scale bar = 50um. (G) Proportion of POU1F1-positive cells in the parenchymal region at E13.5 across the 4 *Dlk1* genotypes. Genotypes were compared using a One-Way ANOVA with Bonferroni's posthoc test comparing each genotype with WT (**p<0.01). (H) Proportion of nuclear HES1-positive cells in the E13.5 pituitary of the 4 *Dlk1* genotypes. Genotypes were compared using a One-Way ANOVA with Bonferroni's posthoc test comparing each genotype with WT (none significant). (I) Left: schematic showing how *Dlk1* might interact with the WNT signalling pathway which promotes commitment towards the *Pou1f1* lineage. Right: RNA scope *in-situ* hybridisation for *Lef1* and *Axin2* in E13.5 pituitary from WT and PAT littermates. *Lef1* and *Axin2*

expression is indicated by pink staining, counterstained in blue (haematoxylin). Scale bar = 100um. (J) Schematic summarising the impact of loss of *Dlk1* expression in the embryonic pituitary gland.

Elevated DLK1 dosage causes increased proliferation of the postnatal AP only when expression is retained in the stem cell compartment.

In postnatal life, overexpression of *Dlk1* from the $TG^{Dlk1\text{-}70C}$ transgene caused an increase in AP volume, but only when WT *Dlk1* expression was retained (compare WT-TG with PAT-TG, Figure 3A). These data suggested that DLK1 produced by marginal zone stem cells and parenchymal cells, might act in concert to promote postnatal proliferation. We consistently observed that WT-TG mice have elevated parenchymal proliferation at P14, the time of maximal expansion of the committed cells prior to puberty (Taniguchi et al. 2001). This increase in proliferation was not observed in the PAT-TG mice (Figure 6A-C). Further, the SOX2+ stem cell compartment is modified in WT-TG and not PAT-TG mice; WT-TG animals at weaning have an increased proportion of SOX2+ cells (Figure 6D, F) and their overall compartmental volume (Figure 6E) in both the MZ and parenchymal clusters is increased. To determine if this translated to an increase in active adult stem cells we performed a stem cell colony-forming assay in adult mice (Andoniadou et al. 2012). In this assay the AP is dissociated and plated at low density in culture media that promotes only the survival of PSCs. The number of colonies after 7 days of culture is indicative of the proportion of active stem cells in the source gland (Figure 6G). In cultures from the AP of 12 week-old WT-TG mice we observed an increase in colony forming units (CFUs) compared to WT littermates, (Figure 5H, I, J) indicating that increasing *Dlk1* expression dosage increases the lifelong stem cell reserve.

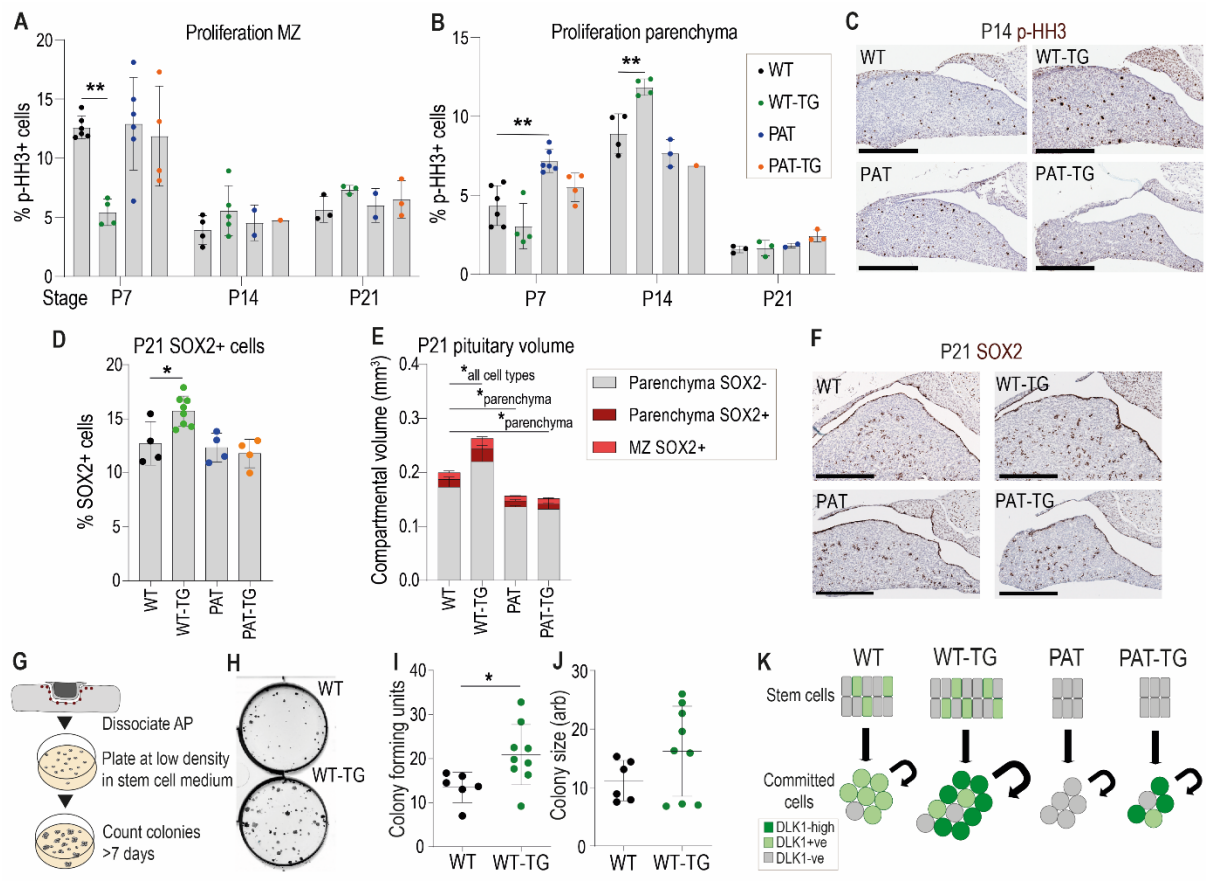

Figure 6. Increased proliferation and stem cell number occurs when Dlk1 dosage is elevated in both stem and parenchymal cells. (A) Proportion of phospho-histone H3 (p-HH3)-positive cells in the marginal zone (MZ) of the anterior pituitary at postnatal days 7, 14 and 21. (B) Proportion of phospho-histone H3 (p-HH3)-positive cells in the parenchymal zone (MZ) of the anterior pituitary at postnatal days 7, 14 and 21. (A) and (B) for each time point genotypes were compared using a One-Way ANOVA with Bonferroni's posthoc test comparing each genotype with WT (**p<0.01). (C) Representative images of immunohistochemistry for p-HH3 at P14 (brown staining, blue counterstain with haemotoxylin), showing increased proportion of positive staining in the parenchyma of the WT-TG anterior pituitary. Scale bars = 250um. (D) Proportion of SOX2-positive cells in the anterior pituitary at postnatal day 21. Genotypes were compared using a One-Way ANOVA with Bonferroni's posthoc test comparing each genotype with WT (*p<0.05). (E) Volumes of P21 anterior pituitaries subdivided into categories dependent on location and SOX2 staining. Genotypes were compared using a 2-Way ANOVA and differ significantly according to genotype ($p < 0.0002$), category ($p < 0.0001$) and the interaction between them ($p<0.0001$). Genotypes are compared in each category to WT using Dunnett's multiple comparison test. WT-TG animals have a significantly increased cell volume in all categories, whereas PAT and PAT-TG animals differ only in parenchymal cell volume (*$p < 0.05$). Bars show mean +/-SD, n = 4-8 animals per genotype. (F) Representative images of immunohistochemistry for SOX2 at P21 (brown staining, blue counterstain with haemotoxylin), showing increased proportion of positive staining in the WT-TG anterior pituitary. Scale bars = 250um. (G) Methodology for determining the number of tissue-resident stem cells in the AP. Whole pituitary is dissected and the posterior lobe removed. The tissue is enzymatically dissociated and counted. A fixed number of cells are seeded at low density into culture media that promotes stem cell growth. After 7 days colonies are counted. Each

colony represents a stem cell from the original organ. (H) Image of pituitary stem cell cultures stained after growth for 7 days, derived from WT (top) and WT-TG (bottom) adult animals. Black dots in the plate indicate colonies derived from a single colony forming unit (CFUs). (I) Number of CFUs from pituitary stem cells following 7 days of culture on 4 separate occasions from a total of n = 6 WT and n = 9 WT-TG, 13-16wk adult animals. (J) Area of CFUs from the stem cell cultures in (I). Genotypes were compared using a Student's t-test, *p<0.05. (K) Schematic summarising the action of *Dlk1* in the different compartments of the AP.

Discussion

We previously demonstrated that adult $TG^{Dlk1\text{-}70C}$ (WT-TG) mice produce more pituitary *Gh* mRNA, have elevated fasting GH levels and concomitant changes to whole-body lipid oxidation pathways (Charalambous et al. 2014). The increase in the GH reserve can be explained by data presented in this study, since adult $TG^{Dlk1\text{-}70C}$ mice have a hypertrophic pituitary gland associated with a ~40% increase in the size of the somatotroph population. We did not observe an increase in linear growth in the WT-TG mice (Figure 4A). This may be explained by the timing of AP volume expansion, which occurs in the third postnatal week (Figure 4B). While we did observe increased circulating GH in WT-TG animals at P21 (Figure S2), this may have been too late to promote the pre-pubertal growth spurt. Moreover, growth signalling by GH requires regulated pulsatile secretion of the hormone (Huang, Huang, and Chen 2019), generated by the homotypic somatotroph cell network (Bonnefont et al. 2005). Future work could investigate how DLK1 dosage-mediated alterations in cell number influences the integrity of this network. In contrast to a role in growth, we have observed that *Dlk1* dosage is elevated during life periods when enhanced peripheral lipid oxidation is beneficial for survival; during suckling (Charalambous et al. 2012) and in the mother during pregnancy (Cleaton et al. 2016). These are periods of life when lipogenesis may be inhibited and tissue fatty acid (FA) oxidation promoted to spare scarce glucose for growth. We speculate that imprinting may be acting on DLK1 dosage to modulate the GH axis and shift the metabolic mode of the organism toward peripheral FA oxidation and away from lipid storage. Therefore, disruption of DLK1 dosage has important consequences for energy homeostasis and metabolic disease.

Dlk1 imprinting is maintained in several embryonic cell populations that take part in the formation of the mature anterior pituitary gland. The endogenous gene is expressed exclusively from the paternally-inherited allele in the ventral diencephalon and in developing Rathke's pouch at E10 (Figure 2D), then in the SOX2+ progenitor populations in mid-late gestation (Figure 3A). As development proceeds, the proportion of DLK1+SOX2+ cells decreases to approximately 10% of all stem cells in the mature gland (Figure 3B-D). Concomitantly, expression of *Dlk1* initiates in committed cells of the parenchyma from their appearance at ~E13.5 (Figure 2D), and is maintained in hormone producing cells, being

particularly abundant in cells of the POU1F1 lineage, somatotrophs (GH+/DLK1+ = 93% of all GH+), lactotrophs (PRL+/DLK1+ = 37% of all PRL+), and thyrotrophs (TSH+/DLK1+ = 40% of all TSH+, Table S1). Indeed, DLK1 shares considerable overlap with POU1F1 in late gestation and may be a direct target of this transcription factor, since three experimentally validated POU1F1 binding sites are located within 120kb of the *Dlk1* gene (Figure S1, (Skowronska-Krawczyk et al. 2014)). Additional experiments, such as measurement of *Dlk1* levels in *Pou1f1*-deleted mice, or targeted deletion of the putative POU1F1 binding sites at the *Dlk1* locus would be required to definitively establish this finding. The expression pattern of *Dlk1* in the progenitor compartment mirrors that of other imprinted genes in the 'Imprinted Growth Network, IGN', such as *Igf2*, *Cdkn1c* and *Grb10* (Scagliotti et al. 2021). These genes have been suggested to comprise the hub of a core pathway that regulates embryonic growth and is progressively deactivated in the perinatal period (Lui et al. 2008; Varrault et al. 2006). The retention of *Dlk1* expression in a small proportion of SOX2+ stem cells in adults suggests heterogeneity of this population, and that a small number of cells retain an embryonic progenitor cell-like phenotype. Well powered analysis of single-cell sequencing datasets of the PSC population over the life course will be required to validate this assertion.

We observed a profound reduction in the volume of the anterior pituitary gland (40-50%) of *Dlk1*-deficient animals at E13.5, before we observed any change in overall body weight (Figure 3B). *Dlk1* is expressed at very high levels in the developing AP compared to other embryonic tissues (compare for example the AP expression with cartilage at E15.5 in Figure2D). The relative volume of the *Dlk1*-deficient AP is maintained at ~40-50% WT levels until the third postnatal week, when there appears to be some catch-up in volume. Importantly and in contrast to the total body weight, addition of the $TG^{Dlk1\text{-}70C}$ transgene does not consistently rescue pituitary volume in *Dlk1*-deficient mice (Figure 3B). These data indicate that loss of *Dlk1* in the SOX2+ progenitors in the early RP causes a persistent reduction to AP volume. Consistently we observed a transient reduction in proliferation of the RP progenitor population at E13.5. This was associated with an increase in the size of the nascent POU1F1+ population, cells which have recently left the dorsal proliferative zone and started along the lineage commitment pathway (Figure 5E, G). This lineage exit is regulated by multiple signalling pathways including the NOTCH and WNT/β-catenin pathways. HES1 is a major downstream transcriptional target of NOTCH in the developing pituitary gland (Goto et al. 2015). Despite robust nuclear expression of HES1 in the RP at E13.5, we saw no difference in the proportion of HES1+ cells between genotypes, suggesting that NOTCH signalling perturbation at this stage is not responsible for pituitary volume reduction in *Dlk1*-deleted embryos. Whether DLK1 is a direct inhibitor of NOTCH signalling is still unresolved, since while some have reported biochemical interactions between DLK1 and NOTCH1

(Baladron et al. 2005), others have failed to co-immunoprecipitate the two proteins in a biologically-relevant context (Wang et al. 2010).

We observed that the expression downstream targets of WNT/β-catenin signalling, *Lef1* and *Axin2*, were increased in expression domain and intensity in PATs. Exit from the proliferating progenitor pool for commitment to the POU1F1 lineage is regulated by an interplay between the transcription factor Prophet of PIT1 (PROP1) and β-catenin binding to and activating the POU1F1 promoter (Olson et al. 2006). Increased activation of β-catenin targets in *Dlk1*-depleted embryos suggests that the normal function of DLK1 may be to act to either reduce WNT production or reduce the sensitivity of cells to the WNT pathway.

The expression of *Dlk1* in both the stem cell and mature hormone-producing compartment of the pituitary gland is perplexing, since it suggests an interaction between DLK1 expression in the progenitor compartment and in the niche. A precedent for this lies in the postnatal neuronal subventricular zone, where DLK1 expression is required in both the stem cells and in niche astrocytes to maintain adult stem cell potency (Ferron et al. 2011). Here we observed that the postnatal WT-TG AP was expanded in volume compared to WT littermates, driven by increased proliferation of the parenchymal cells in the second postnatal week. A similar volume expansion was not observed when PAT-TG animals were compared to PAT littermates (Figure 4C, 6B). These data suggest that excess *Dlk1* can promote pituitary hypertrophy, but only if DLK1 is expressed in the SOX2+ compartment when dosage is increased in the parenchyma. Intriguingly, the increase in cell division mediated by excess DLK1 at P14 is in the parenchyma, and therefore DLK1 is not acting cell autonomously in stem cells to promote proliferation, yet SOX2+DLK1+ cells are required for volume expansion. This suggests that the SOX2+DLK1+ cells may produce a signal that promotes parenchymal proliferation, analogous to previous data where we demonstrated that the postnatal stem cells promote committed cell proliferation by a WNT-mediated pathway (Russell et al. 2021). We speculate that DLK1 production from stem cells might comprise part of this paracrine signalling system that is required for the size regulation of the mature pituitary gland. In concert, increased expression of DLK1 in the parenchyma might alter the sensitivity of cells to proliferative signals.

Finally, we observed that the SOX2+ stem cell compartment was expanded in the WT-TG but not PAT-TG postnatal and adult pituitary gland. This increase in stem cell number may be a result of 'sparing' of stem cell proliferation earlier in development, since WT-TG pituitaries have significantly fewer dividing cells in the marginal zone at P7. Regardless, the overall effect of increased DLK1 dosage is to increase overall AP volume and increase the size of the stem cell population.

In conclusion, we have shown that DLK1 is an important determinant of anterior pituitary size, and acts at multiple stages of development to modulate proliferative populations. The consequences of altered *Dlk1* dosage in the pituitary affect hormone production throughout life.

Methods

Mice. All animal procedures were carried out in accordance with the recommendations provided in the Animals (Scientific procedures) Act 1986 of the UK Government. Mice were maintained on a 12-hour light : dark cycle in a temperature and humidity-controlled room and re-housed in clean cages weekly. All mice were fed *ad libitum* and given fresh tap water daily. Mice were weaned at postnatal day (P) 21, or a few days later if particularly small. Thereafter, they were housed in single-sex groups (5 per cage maximum) or occasionally singly housed. Embryos were generated through timed matings (either as a pair or a trio). Noon on the day of the vaginal plug was considered as embryonic day (E)0.5.

All mice were maintained on a C57BL6/J background. The generation of the *Dlk1*-knockout (*Dlk1*^{tm1Srba}) and the *Dlk1*-TG BAC transgenic (Tg$^{Dlk1\text{-}70C}$) lines has been previously described (Raghunandan et al. 2008; da Rocha et al. 2009). For colony maintenance maternal heterozygotes (*Dlk1*$^{tm1Srbpa/+}$, hereafter called *Dlk1*$^{-/+}$ or MAT) and littermate wild-type (*Dlk1*$^{+/+}$, WT) animals were generated. *Tg*$^{Dlk1\text{-}70C}$ (WT-TG) animals were maintained as heterozygotes by crossing WT females with heterozygous WT-TG males. *Dlk1*$^{+/tm1Srbpa}$ (hereafter called *Dlk1*$^{+/-}$ or PAT) and littermate WT animals or embryos were generated by crossing WT females with MAT males. *Dlk1*$^{+/tm1Srbpa}$; *Tg*$^{Dlk1\text{-}70C}$ (PAT-TG) animals or embryos were obtained by crossing WT-TG females with MAT males. From these crosses, WT, PAT, and WT-TG littermates were also generated (shown in Fig2A).

Genotyping and *Dlk1* isoform analysis. Genotyping was performed on ear and embryonic tail biopsies with DNA extracted using DNAReleasy (LS02, Anachem). *Dlk1* isoform analysis was performed on cDNA from E18.5 pituitary glands, synthesised as described below. PCR was performed using REDTaq® ReadyMix™ PCR Reaction Mix (R2523, Merck-SIGMA) using previously published primers (Charalambous et al. 2014).

RNA extraction and cDNA synthesis. RNA from pituitary glands of E18.5 embryos and adults was extracted using TRIzol™ LS (10296028, Invitrogen™) and treated with DNase I (M0303, New England Biolabs (NEB)), following the manufacturer's instructions. Complementary DNA (cDNA) was obtained by Reverse Transcription (RT) using 200-300 ng of purified RNA as template and Moloney Murine Leukemia Virus (M-MuLV) Reverse Transcriptase (M0253, NEB). cDNA was synthesised using the standard first strand synthesis protocol with random hexamers (S1230, NEB).

Histology. Fresh embryos and postnatal pituitaries were fixed with 4% w/v paraformaldehyde (PFA, P6148, Merck-SIGMA) in Phosphate-Buffered Saline (PBS, BR0014G, Thermo Scientific Oxoid) or Neutral Buffered Formalin (Merck-SIGMA, HT501128) overnight at 4°C and dehydrated through an increasing ethanol series the following day. Samples were stored at 4°C in 70% ethanol or dehydrated to 100% ethanol the day before the paraffin embedding. On the day of embedding, samples were incubated at room temperature (RT) with Histoclear II (National Diagnostics, HS202) (2 x 20 minutes for E9.5-E11.5 and postnatal pituitaries, 2 x 35 minutes for E13.5) or Xylene (VWR) (2 x 45 minutes for E15.5, 2 x 1 hour for E18.5). This was followed by 3 x 1-hour incubations at 65°C with Histosec® (1.15161.2504, VWR). 5µm histological sections were cut using a Thermo HM325 microtome, mounted

on Menzel-Gläser Superfrost®Plus slides (Thermo Scientific, J1810AMNZ) and used for *in situ* hybridisation (ISH), RNAscope, immunohistochemistry (IHC) and immunofluorescence (IF).

mRNA *in situ* hybridisation. ISH was performed as previously described (Giri et al. 2017). Sections were hybridised overnight at 65°C with sense and antisense digoxigenin (DIG)-riboprobes against *Dlk1* (da Rocha et al. 2009). Sections were washed and incubated overnight at 4°C with anti-Digoxigenin-AP antibody (45-11093274910 Merck-SIGMA, 1:1000). Staining was achieved by adding a solution of 4-Nitro blue tetrazolium chloride (NBT, 11383213001, Merck-SIGMA) and 5-Bromo-4-chloro-3-indolyl phosphate disodium salt (BCIP, 11383221001, Merck-SIGMA). Sections were mounted using DPX (6522, Merck-SIGMA). Sense controls for each probe were tested at E13.5 and showed no staining under identical conditions.

RNAScope mRNA *in situ* hybridisation. RNAScope experiments were performed as previously described (Russell et al. 2021). For the expression analysis of early developmental markers, mRNA expression was assessed using the RNAScope singleplex chromogenic kits (Advanced Cell Diagnostics) on NBF fixed paraffin embedded sections processed as described in the previous section. The probes used for this experiment are listed in Table S5. ImmEdge Hydrophobic Barrier PAP Pen (H-4000, Vector Laboratories) was used to draw a barrier around section while air-drying following the first ethanol washes. Sections were counterstained with Mayer's Haematoxylin (Vector Laboratories, H-3404), left to dry at 60°C for 30 min before mounting with VectaMount Permanent Mounting Medium (Vector Laboratories, H-5000).

Immunohistochemistry and immunofluorescence. IHC on histological sections was performed as previously described (Giri et al. 2017). For IHC, unmasking was achieved by boiling the histological sections with 10 mM tri-sodium citrate buffer pH 6 for 20 minutes. Detection of the proteins was achieved by incubating the histological sections overnight at 4 °C with the primary antibodies described in Table S6, and detected with secondary biotinylated goat α-rabbit, goat α-mouse or α -goat secondary (BA-1000, BA-9200 and BA9500, Vector Laboratories, 1:300), followed by 1-hour incubation at room temperature with Vectastain® Elite ABC-HRP kit (PK-6100, Vector Laboratories). Staining was achieved through colorimetric reaction using DAB Peroxidase Substrate Kit (SK-4100, Vector Laboratories). Slides were lightly counterstained with Mayer's Haematoxylin (MHS16, Merck-SIGMA) and mounted using DPX. For double IF, unmasking was achieved as described above, but the Tris-EDTA buffer pH 9 [10 mM Tris Base, 1 mM EDTA, 0.05% Tween 20]. Histological sections were incubated overnight at 4°C with the primary antibody, incubated sequentially with a goat biotinylated anti-rabbit (1:200) then with streptavidin-594 (SA5594, Vector Laboratories, 1:200) at RT. The second primary was added to the sections overnight at 4°C then detected with a goat α-rabbit DyLight® 488 (DI1488, Vector Laboratories, 1:200) and mounted using VECTASHIELD® Antifade Mounting Medium with DAPI (H-1200-10, Vector Laboratories). Isotype controls for each antibody showed no staining under identical conditions.

Stereological estimation of pituitary volumes. Pituitary volume was estimated using the Cavallieri method (Howard and Reed 1998). Briefly, the pituitary was exhaustively sectioned then sections were collected at regular, non-overlapping intervals throughout the gland from a random starting point and stained with H&E. Images of each H&E-stained section were acquired using a NanoZoomer HT (Hamamatsu) and processed using NDP.view2 software (Hamamatsu) to calculate the pituitary area at least 20 times per pituitary, which was then converted to volume. Samples were blinded prior to counting.

Cell counting. Histological sections were immunostained as described above and imaged using the NanoZoomer HT (Hammamatsu). Images were exported using NDP.view2 and cell counted using the cell counter plugin in ImageJ (Schindelin et al. 2012). For IHC, cells that exhibited a clear brown staining were manually counted as positive. Samples were blinded prior to counting. Total number of cells was calculated by counting haematoxylin-counterstained cells. For IF, cells that exhibited a clear fluorescence signal were manually counted as positive. Total number of cells was calculated by counting DAPI-counterstained cells.

Imaging. Images of histological sections were acquired using a NanoZoomer HT (Hammamatsu). Fluorescence images and higher magnification bright-field images were acquired using a Zeiss Axioplan II microscope with a Luminera 3 digital camera and INFINITY ANALYSE software v6.5.6 (Luminera). Images were combined using Adobe Photoshop 23.4.1 release 2022 (Adobe).

Analyses of single cell and single nuclei RNA-seq data. Single-cell sequencing data from the mouse pituitary gland was downloaded from GEO using accession numbers GSE120410 (postnatal day 4, P4) and GSE142074 (postnatal day 49, P49) and analysed as previously described (Scagliotti et al. 2021).

Human single-nuclei RNA sequencing pituitary data was obtained from GEO accession number GSE178454. Using Seurat (v4.1.0) (Satija et al. 2015), (Macosko et al. 2015), (Stuart et al. 2019), (Hao et al. 2021) in R, cells from male and female datasets of all ages were taken forward if they expressed between 1000–5500 genes and <10% mitochondrial transcripts, removing doublets and low-quality cells. All 6 filtered datasets were integrated using the SCTransform workflow (Hafemeister and Satija 2019). Clustering and visualisation for the integrated objects were carried out using the the default resolution and 1:15 principal components. Clusters were named according to known cell-type markers as previously reported (Cheung et al. 2018), (Zhang et al. 2022), (Scagliotti et al. 2021).

For both mouse and human data, *Dlk1/DLK1* expression was plotted in the respective datasets using the "FeaturePlot" function in Seurat with a min.cutoff = 0 and split.by = 'Age'. Percentage of stem cells expressing *Dlk1/DLK1* was calculated under the 'integrated' assay of the Seurat object using the WhichCells function of grouped 'Stem Cells' expressing *Dlk1/DLK1*.

Mapping POU1F1 binding sites to the mouse *Dlk1* region. POU1F1 binding sites identified using chromatin immunoprecipitation followed by sequencing (ChiP-seq) in growth hormone (GH)-expressing rat pituitary cell line were obtained from a published dataset (Skowronska-Krawczyk et al. 2014). POU1F1 binding sites overlapping the rat *Dlk1* locus (chr6: 133828590-134274323, rn4 assembly) were selected and converted to the orthologues region on mouse chr12 (mm10 assembly) using University of California Santa Cruz Genomics Institute Genome Browser (UCSC). The reported POU1F1 binding sites displayed a rat/mouse sequence conservation higher than 98%. Data were visualised using Gviz R package (Hahne and Ivanek 2016).

Western blotting. Sample preparation, gel electrophoresis and western blotting were described previously (da Rocha et al. 2009), with Abcam anti-DLK1 (ab21682, which recognises the intracellular domain of the protein) at 1:500. Anti-alpha tubulin (Merck-SIGMA, clone B-5-1-2) was used as a loading control at 1:10000.

Pituitary SC cultures. Pituitary stem cells were isolated from anterior pituitaries collected from adult female mice at 13-16 weeks of age, essentially as described in Andoniadou, 2013 (Andoniadou et al. 2013). Briefly, mice were culled by CO_2 asphyxiation, the skin overlying the skull cut and the skull bone opened with scissors. Using a dissecting microscope, the brain was carefully removed, as well as the

posterior lobe of the pituitary gland. The remaining anterior pituitary was gently detached and transferred to a 1.5 ml microcentrifuge tube containing 200 µl of enzyme mix [0.5% w/v Collagenase type II (Worthington), 50 µg/ml DNase (Worthington), 2.5 µg/ml Fungizone (Gibco) and 0.1% v/v trypsin-EDTA solution 0.05% (Gibco) in Hank's Balanced Salt Solution (HBSS, Gibco)]. Once transferred, the anterior pituitary was incubated at 37°C for up to 4 hours, under gentle agitation. Following the incubation, samples were mechanically dissociated into single cell suspensions by vigorously pipetting the solution up and down. 1 ml of HBSS was added to the solution to dilute the enzyme mix and samples were centrifuged at 2500 rpm for 5 minutes. The cell pellet was re-suspended in Ultraculture Medium (Lonza), supplemented with 5% v/v fetal bovine serum (FBS, Invitrogen), 1% v/v penicillin/streptomycin (P/S, Merck-SIGMA), 20 ng/ml basic fibroblast growth factor (bFGF, R&D) and 50 ng/ml Cholera Toxin (Merck-SIGMA). Cells were counted using a haemocytometer, upon incubation with an equal volume of Trypan blue solution 0.4% (Merck-SIGMA) to assess cell viability. Viable cells were then plated at a density of 1000 cells/cm^2 and fresh media replaced every three days.

Plasma GH determination. ELISA kits were used for measurements Growth Hormone (Merck-SIGMA EZRMGH-45K) according to manufacturers' instructions.

Timing of puberty. Day of puberty was determined as the time of first vaginal opening (VO) in postnatal female mice. Animals were checked daily in the morning from P18 to P35 and the first appearance of VO and body weight on that day recorded. For this experiment all mice were weaned at P21.

Statistical analysis. All statistical tests were performed using the GraphPad Prism Software version 9 for Windows, GraphPad Software, San Diego California USA, www.graphpad.com. Specific tests, significance values and number of samples analysed are indicated in the respective figure/table legends, and all error bars represent the standard deviation (SD). Data points in graphs represent individual animals as biological replicates. Outliers were removed using Grubb's test within the Prism application.

SupplementaryTables

		WT			WT-TG		
Cell	*Subgroup*	*Mean*	*SD*	*n*	*Mean*	*SD*	*n*
GH+	**Total proportion**	**0.290**	**0.023**	7	**0.294**	**0.020**	7
	DLK1-/GH+	0.019	0.003		0.014	0.002	
	DLK1+/GH+	0.271	0.008		0.280	0.007	
	% co-stained DLK1	*93*			*95*		
PRL+	**Total proportion**	**0.213**	**0.012**	4	**0.201**	**0.018**	4
	DLK1-/PRL+	0.135	0.003		0.130	0.011	
	DLK1+/PRL+	0.078	0.004		0.072	0.002	
	% co-stained DLK1	*37*			*36*		
TSH+	**Total proportion**	**0.096**	**0.011**	4	**0.091**	**0.010**	4
	TSH+	0.057	0.004		0.056	0.004	
	DLK1+/TSH+	0.038	0.002		0.035	0.002	
	% co-stained DLK1	*40*			*38*		
FSH+	**Total proportion**	**0.096**	**0.013**	2	**0.092**	**0.000**	2
	FSH +ve	0.077	0.011		0.074	0.001	
	DLK1+/FSH+	0.018	0.002		0.018	0.002	
	% co-stained DLK1	*19*			*20*		
ACTH+	**Total proportion**	**0.130**	**0.010**	4	**0.109**	**0.016**	4
	ACTH+	0.129	0.005		0.109	0.008	
	DLK1+/ACTH+	0.000	0.000		0.000	0.000	
	% co-stained DLK1	*0*			*0*		
	Unclassified	**0.177**			**0.213**		

Table S1. Proportions of AP cells labelled with hormonal markers in WT and WT-TG female animals at 12 weeks of age.

	Genotype	Total body mass (g)				
		Mean	*SD*	*n*	*p vs WT*	*p vs PAT*
E11.5	WT	0.0464	0.0043	11		
	WT-TG	0.0458	0.0043	11	ns	
	PAT	0.0444	0.0043	8	ns	
	PAT-TG	0.0433	0.0081	7	ns	ns
E13.5	WT	0.1447	0.0136	7		
	WT-TG	0.1381	0.0157	17	ns	
	PAT	0.1468	0.0111	16	ns	
	PAT-TG	0.1464	0.0181	10	ns	ns
E18.5	WT	1.2062	0.1311	24		
	WT-TG	1.2110	0.1060	32	ns	
	PAT	1.0205	0.0711	15	<0.0001	
	PAT-TG	1.1107	0.0808	20	0.0125	0.0513
P7	WT	4.0329	0.2682	7		
	WT-TG	3.8280	0.2197	5	ns	
	PAT	3.0933	0.2542	9	0.0003	
	PAT-TG	3.7730	0.5926	10	ns	0.0038
P14	WT	7.8124	0.6887	17		
	WT-TG	8.6843	0.6171	7	0.0161	
	PAT	5.6000	0.6420	8	<0.0001	
	PAT-TG	6.7640	0.2463	5	0.0097	0.0105
P21	WT	10.7120	1.6084	10		
	WT-TG	11.0489	1.1016	9	ns	
	PAT	8.8117	1.0644	6	0.0129	ns
	PAT-TG	10.1354	0.7752	13	ns	

Table S2. Total body mass of animals from matched litters sacrificed from E11.5 to P21. Individuals in each age group were compared by One-Way ANOVA with post-hoc pairwise testing WT vs WT-TG, PAT, PAT-TG and PAT vs PAT-TG, corrected for multiple comparisons using Bonferroni's adjustment.

	Genotype	AP Volume (mm^3)				PP Volume (mm^3)				
		Mean	*SD*	*p vs WT*	*p vs PAT*	*Mean*	*SD*	*p vs WT*	*p vs PAT*	*n*
E13.5	WT	0.0269	0.0056			0.0022	0.0005			9
	WT-TG	0.0255	0.0043	ns		0.0023	0.0004	ns		11
	PAT	0.0164	0.0011	<0.0001		0.0019	0.0002	ns		6
	PAT-TG	0.0172	0.0022	<0.0001	ns	0.0021	0.0022	ns	ns	8
E18.5	WT	0.0600	0.0084			0.0092	0.0006			7
	WT-TG	0.0664	0.0059	ns		0.0096	0.0006	ns		5
	PAT	0.0444	0.0094	0.0025		0.0102	0.0016	ns		7
	PAT-TG	0.0479	0.0044	0.1670	ns	0.0097	0.0020	ns	ns	8

Table S3A. Pituitary volumes acquired by stereological estimation in the embryo.

	Genotype	AL Volume (mm^3)				IL Volume (mm^3)				PL Volume (mm^3)				
		Mean	*SD*	*p vs WT*	*p vs PAT*	*Mean*	*SD*	*p vs WT*	*p vs PAT*	*Mean*	*SD*	*p vs WT*	*p vs PAT*	*n*
P7	WT	0.0783	0.0069			0.0169	0.0020			0.0159	0.0022			5
	WT-TG	0.0817	0.0065	ns		0.0157	0.0019	ns		0.0165	0.0024	ns		4
	PAT	0.0406	0.0070	<0.0001		0.0110	0.0020	0.0014		0.0138	0.0036	ns		8
	PAT-TG	0.0565	0.0097	0.0010	0.0074	0.0143	0.0034	ns	ns	0.0157	0.0030	ns	ns	5
P14	WT	0.1601	0.0286			0.0221	0.0029			0.0244	0.0031			6
	WT-TG	0.1795	0.0306	ns		0.0252	0.0034	ns		0.0249	0.0044	ns		7
	PAT	0.0857	0.0159	0.0007		0.0229	0.0018	ns		0.0168	0.0010	ns		5
	PAT-TG	0.0894	0.0165	0.0046	ns	0.0225	0.0025	ns	ns	0.0196	0.0041	ns	ns	3
P21	WT	0.1972	0.0252			0.0361	0.0036			0.0317	0.0047			6
	WT-TG	0.2617	0.0494	0.0105		0.0359	0.0076	0.0268		0.0348	0.0044	ns		8
	PAT	0.1542	0.0043	ns		0.0301	0.0089	ns		0.0376	0.0088	ns		3
	PAT-TG	0.1549	0.0257	ns	ns	0.0234	0.0030	ns	ns	0.0251	0.0030	ns	ns	7

Table S3B. Pituitary volumes acquired by stereological estimation in of the intact adult gland. Individuals in each age group were compared by One-Way ANOVA with post-hoc pairwise testing WT vs WT-TG, PAT, PAT-TG and PAT vs PAT-TG, corrected for multiple comparisons using Bonferroni's adjustment.

	Genotype	CL % p-HH3		NC % p-HH3		Total % p-HH3		
		Mean	*SD*	*Mean*	*SD*	*Mean*	*SD*	*n*
E11.5	WT	-	-	-	-	5.59	1.04	5
	WT-TG	-	-	-	-	6.56	1.26	4
	PAT	-	-	-	-	6.80	2.89	4
	PAT-TG	-	-	-	-	7.02	2.27	4
E13.5	WT	24.34	3.42	4.01	1.91	11.77	3.09	7
	WT-TG	24.29	2.68	4.71	1.29	12.49	2.88	8
	PAT	19.89	2.28	3.53	1.04	9.69	0.85	7
	PAT-TG	18.85	2.48	2.95	0.78	9.06	1.36	8
E18.5	WT	10.34	1.43	8.46	0.43	8.94	0.30	5
	WT-TG	10.56	2.26	8.42	2.10	8.97	2.00	7
	PAT	10.64	2.91	8.76	3.66	9.25	3.42	8
	PAT-TG	11.19	2.86	11.02	3.50	11.01	3.20	8
P7	WT	12.71	1.22	4.58	1.63	5.15	1.59	6
	WT-TG	5.73	1.15	2.33	0.25	2.55	0.29	3
	PAT	12.91	3.91	7.17	0.73	7.59	0.86	6
	PAT-TG	11.87	4.22	5.50	0.90	5.94	0.63	4
P14	WT	3.92	1.22	9.18	1.25	8.91	1.24	4
	WT-TG	5.56	2.11	11.32	0.95	11.52	0.87	5
	PAT	4.54	1.51	7.70	0.79	7.66	0.87	3
	PAT-TG	4.76	nd	6.97	nd	6.87	nd	1
P21	WT	5.66	1.09	1.57	0.22	1.82	0.25	3
	WT-TG	7.35	0.36	1.65	0.49	2.07	0.47	3
	PAT	6.01	1.44	1.81	0.15	2.04	0.20	2
	PAT-TG	6.52	1.58	2.42	0.37	2.70	0.46	3

Table S4. Proportion of proliferating cells (IHC positive for p-HH3) in the embryonic and postnatal pituitary gland.

Probe target	Cat#	Source
Mm-Lef1	441861	ACDBio
Mm-Axin2	400331	ACDBio
Mm-Shh	314361	ACDBio
Mm-Fgf8	313411	ACDBio
Mm-Fgf10	446371	ACDBio

712 **Table S5.** RNAScope probes used in this study

713

Antibody target (species)	Source	Antibody titre
DLK1 (mouse, WB)	Abcam ab21682	1:500
DLK1 (mouse, IHC)	R&D AF8277	1:200
DLK1 (mouse, IHC)	Abcam ab210471	1:1000
Alpha tubulin (human, WB)	Merck-SIGMA T5168	1:10,000
GH (Rat)	National Hormone and Peptide Program (NHPP)	1:1000
PRL (Mouse)		1:500
TSHβ (Rat)		1:500
FSHβ (Rat)		1:500
ACTH (Rat)		1:1000
LH (Rat)		1:500
POU1F1 (Mouse)	A gift from S. Rhodes, Indiana University School of Medicine, Indianapolis USA	1:300
SOX2 (Mouse)	Abcam ab92494	1:400
α-phospho-Histone H3-Ser10 (human)	Merck-SIGMA 06-570	1:300
HES1 (human)	Cell Signaling Technologies D6P2U	1:300
Goat SOX2	R&D AF2018	1:300

714 **Table S6** Primary antibodies used in the study.

715

Acknowledgements

We thank Prof Anne Ferguson-Smith, University of Cambridge for the *TG*$^{Dlk1\text{-}70C}$ mouse line. Funding was provided by the Medical Research Council (MRC) Grants MR/L002345/1 (MC), MR/R022836/1 (MC) and MR/T012153/1 (CLA), and the Society for Endocrinology, UK (MH). MLV was supported by a studentship from the NIHR Biomedical Research Centre at Guy's and St Thomas' NHS Foundation Trust and King's College London. TLW was funded by King's College London as part of the "Cell Therapies and Regenerative Medicine" Four-Year Welcome Trust PhD Training Program. CGM was sponsored by Action Medical Research (GN2272) and Barts Charity (GN 417/2238 & MGU0551).

Competing interests

We have no competing interests to declare.

References

Andoniadou, C. L., C. Gaston-Massuet, R. Reddy, R. P. Schneider, M. A. Blasco, P. Le Tissier, T. S. Jacques, L. H. Pevny, M. T. Dattani, and J. P. Martinez-Barbera. 2012. 'Identification of novel pathways involved in the pathogenesis of human adamantinomatous craniopharyngioma', *Acta Neuropathol*, 124: 259-71.

Andoniadou, C. L., D. Matsushima, S. N. Mousavy Gharavy, M. Signore, A. I. Mackintosh, M. Schaeffer, C. Gaston-Massuet, P. Mollard, T. S. Jacques, P. Le Tissier, M. T. Dattani, L. H. Pevny, and J. P. Martinez-Barbera. 2013. 'Sox2(+) stem/progenitor cells in the adult mouse pituitary support organ homeostasis and have tumor-inducing potential', *Cell Stem Cell*, 13: 433-45.

Appelbe, O. K., A. Yevtodiyenko, H. Muniz-Talavera, and J. V. Schmidt. 2013. 'Conditional deletions refine the embryonic requirement for Dlk1', *Mech Dev*, 130: 143-59.

Baladron, V., M. J. Ruiz-Hidalgo, M. L. Nueda, M. J. Diaz-Guerra, J. J. Garcia-Ramirez, E. Bonvini, E. Gubina, and J. Laborda. 2005. 'dlk acts as a negative regulator of Notch1 activation through interactions with specific EGF-like repeats', *Exp Cell Res*, 303: 343-59.

Bonnefont, X., A. Lacampagne, A. Sanchez-Hormigo, E. Fino, A. Creff, M. N. Mathieu, S. Smallwood, D. Carmignac, P. Fontanaud, P. Travo, G. Alonso, N. Courtois-Coutry, S. M. Pincus, I. C. Robinson, and P. Mollard. 2005. 'Revealing the large-scale network organization of growth hormone-secreting cells', *Proc Natl Acad Sci U S A*, 102: 16880-5.

Camper, S. A., T. L. Saunders, R. W. Katz, and R. H. Reeves. 1990. 'The Pit-1 transcription factor gene is a candidate for the murine Snell dwarf mutation', *Genomics*, 8: 586-90.

Charalambous, M., S. T. Da Rocha, E. J. Radford, G. Medina-Gomez, S. Curran, S. B. Pinnock, S. R. Ferron, A. Vidal-Puig, and A. C. Ferguson-Smith. 2014. 'DLK1/PREF1 regulates nutrient metabolism and protects from steatosis', *Proc Natl Acad Sci U S A*, 111: 16088-93.

Charalambous, M., S. R. Ferron, S. T. da Rocha, A. J. Murray, T. Rowland, M. Ito, K. Schuster-Gossler, A. Hernandez, and A. C. Ferguson-Smith. 2012. 'Imprinted gene dosage is critical for the transition to independent life', *Cell Metab*, 15: 209-21.

Cheung, L. Y. M., and S. A. Camper. 2020. 'PROP1-Dependent Retinoic Acid Signaling Regulates Developmental Pituitary Morphogenesis and Hormone Expression', *Endocrinology*, 161.

Cheung, L. Y. M., A. S. George, S. R. McGee, A. Z. Daly, M. L. Brinkmeier, B. S. Ellsworth, and S. A. Camper. 2018. 'Single-Cell RNA Sequencing Reveals Novel Markers of Male Pituitary Stem Cells and Hormone-Producing Cell Types', *Endocrinology*, 159: 3910-24.

Cheung, L. Y., K. Rizzoti, R. Lovell-Badge, and P. R. Le Tissier. 2013. 'Pituitary phenotypes of mice lacking the notch signalling ligand delta-like 1 homologue', *J Neuroendocrinol*, 25: 391-401.

Cleaton, M. A., C. L. Dent, M. Howard, J. A. Corish, I. Gutteridge, U. Sovio, F. Gaccioli, N. Takahashi, S. R. Bauer, D. S. Charnock-Jones, T. L. Powell, G. C. Smith, A. C. Ferguson-Smith, and M. Charalambous. 2016. 'Fetus-derived DLK1 is required for maternal metabolic adaptations to pregnancy and is associated with fetal growth restriction', *Nat Genet*, 48: 1473-80.

da Rocha, S. T., M. Charalambous, S. P. Lin, I. Gutteridge, Y. Ito, D. Gray, W. Dean, and A. C. Ferguson-Smith. 2009. 'Gene dosage effects of the imprinted delta-like homologue 1 (dlk1/pref1) in development: implications for the evolution of imprinting', *PLoS Genet*, 5: e1000392.

da Rocha, S. T., M. Tevendale, E. Knowles, S. Takada, M. Watkins, and A. C. Ferguson-Smith. 2007. 'Restricted co-expression of Dlk1 and the reciprocally imprinted non-coding RNA, Gtl2: implications for cis-acting control', *Dev Biol*, 306: 810-23.

Dauber, A., M. Cunha-Silva, D. B. Macedo, V. N. Brito, A. P. Abreu, S. A. Roberts, L. R. Montenegro, M. Andrew, A. Kirby, M. T. Weirauch, G. Labilloy, D. S. Bessa, R. S. Carroll, D. C. Jacobs, P. E. Chappell, B. B. Mendonca, D. Haig, U. B. Kaiser, and A. C. Latronico. 2017. 'Paternally Inherited DLK1 Deletion Associated With Familial Central Precocious Puberty', *J Clin Endocrinol Metab*, 102: 1557-67.

Davis, S. W., A. H. Mortensen, and S. A. Camper. 2011. 'Birthdating studies reshape models for pituitary gland cell specification', *Dev Biol*, 352: 215-27.

Ferron, S. R., M. Charalambous, E. Radford, K. McEwen, H. Wildner, E. Hind, J. M. Morante-Redolat, J. Laborda, F. Guillemot, S. R. Bauer, I. Farinas, and A. C. Ferguson-Smith. 2011. 'Postnatal loss of Dlk1 imprinting in stem cells and niche astrocytes regulates neurogenesis', *Nature*, 475: 381-5.

Giri, D., M. L. Vignola, A. Gualtieri, V. Scagliotti, P. McNamara, M. Peak, M. Didi, C. Gaston-Massuet, and S. Senniappan. 2017. 'Novel FOXA2 mutation causes Hyperinsulinism, Hypopituitarism with Craniofacial and Endoderm-derived organ abnormalities', *Hum Mol Genet*, 26: 4315-26.

781 Gorkin, D. U., I. Barozzi, Y. Zhao, Y. Zhang, H. Huang, A. Y. Lee, B. Li, J. Chiou, A. Wildberg, B. Ding, B. Zhang,
782 M. Wang, J. S. Strattan, J. M. Davidson, Y. Qiu, V. Afzal, J. A. Akiyama, I. Plajzer-Frick, C. S. Novak, M.
783 Kato, T. H. Garvin, Q. T. Pham, A. N. Harrington, B. J. Mannion, E. A. Lee, Y. Fukuda-Yuzawa, Y. He,
784 S. Preissl, S. Chee, J. Y. Han, B. A. Williams, D. Trout, H. Amrhein, H. Yang, J. M. Cherry, W. Wang, K.
785 Gaulton, J. R. Ecker, Y. Shen, D. E. Dickel, A. Visel, L. A. Pennacchio, and B. Ren. 2020. 'An atlas of
786 dynamic chromatin landscapes in mouse fetal development', *Nature*, 583: 744-51.
787 Goto, M., M. Hojo, M. Ando, A. Kita, M. Kitagawa, T. Ohtsuka, R. Kageyama, and S. Miyamoto. 2015. 'Hes1 and
788 Hes5 are required for differentiation of pituicytes and formation of the neurohypophysis in pituitary
789 development', *Brain Res*, 1625: 206-17.
790 Hafemeister, C., and R. Satija. 2019. 'Normalization and variance stabilization of single-cell RNA-seq data using
791 regularized negative binomial regression', *Genome Biol*, 20: 296.
792 Hahne, F., and R. Ivanek. 2016. 'Visualizing Genomic Data Using Gviz and Bioconductor', *Methods Mol Biol*,
793 1418: 335-51.
794 Hao, Y., S. Hao, E. Andersen-Nissen, W. M. Mauck, 3rd, S. Zheng, A. Butler, M. J. Lee, A. J. Wilk, C. Darby, M.
795 Zager, P. Hoffman, M. Stoeckius, E. Papalexi, E. P. Mimitou, J. Jain, A. Srivastava, T. Stuart, L. M.
796 Fleming, B. Yeung, A. J. Rogers, J. M. McElrath, C. A. Blish, R. Gottardo, P. Smibert, and R. Satija.
797 2021. 'Integrated analysis of multimodal single-cell data', *Cell*, 184: 3573-87 e29.
798 Hovanes, K., T. W. Li, J. E. Munguia, T. Truong, T. Milovanovic, J. Lawrence Marsh, R. F. Holcombe, and M. L.
799 Waterman. 2001. 'Beta-catenin-sensitive isoforms of lymphoid enhancer factor-1 are selectively
800 expressed in colon cancer', *Nat Genet*, 28: 53-7.
801 Howard, Vyvyan, and M. G. Reed. 1998. *Unbiased stereology : three-dimensional measurement in microscopy*
802 (Springer: New York).
803 Huang, L., Z. Huang, and C. Chen. 2019. 'Rhythmic growth hormone secretion in physiological and pathological
804 conditions: Lessons from rodent studies', *Mol Cell Endocrinol*, 498: 110575.
805 Ioannides, Y., K. Lokulo-Sodipe, D. J. Mackay, J. H. Davies, and I. K. Temple. 2014. 'Temple syndrome:
806 improving the recognition of an underdiagnosed chromosome 14 imprinting disorder: an analysis of 51
807 published cases', *J Med Genet*, 51: 495-501.
808 Jho, E. H., T. Zhang, C. Domon, C. K. Joo, J. N. Freund, and F. Costantini. 2002. 'Wnt/beta-catenin/Tcf signaling
809 induces the transcription of Axin2, a negative regulator of the signaling pathway', *Mol Cell Biol*, 22:
810 1172-83.
811 Larsen, J. B., C. H. Jensen, H. D. Schroder, B. Teisner, P. Bjerre, and C. Hagen. 1996. 'Fetal antigen 1 and
812 growth hormone in pituitary somatotroph cells', *Lancet*, 347: 191.
813 Li, S., E. B. Crenshaw, 3rd, E. J. Rawson, D. M. Simmons, L. W. Swanson, and M. G. Rosenfeld. 1990. 'Dwarf
814 locus mutants lacking three pituitary cell types result from mutations in the POU-domain gene pit-1',
815 *Nature*, 347: 528-33.
816 Lui, J. C., G. P. Finkielstain, K. M. Barnes, and J. Baron. 2008. 'An imprinted gene network that controls
817 mammalian somatic growth is down-regulated during postnatal growth deceleration in multiple organs',
818 *Am J Physiol Regul Integr Comp Physiol*, 295: R189-96.
819 Macosko, E. Z., A. Basu, R. Satija, J. Nemesh, K. Shekhar, M. Goldman, I. Tirosh, A. R. Bialas, N. Kamitaki, E.
820 M. Martersteck, J. J. Trombetta, D. A. Weitz, J. R. Sanes, A. K. Shalek, A. Regev, and S. A. McCarroll.
821 2015. 'Highly Parallel Genome-wide Expression Profiling of Individual Cells Using Nanoliter Droplets',
822 *Cell*, 161: 1202-14.
823 Olson, L. E., J. Tollkuhn, C. Scafoglio, A. Krones, J. Zhang, K. A. Ohgi, W. Wu, M. M. Taketo, R. Kemler, R.
824 Grosschedl, D. Rose, X. Li, and M. G. Rosenfeld. 2006. 'Homeodomain-mediated beta-catenin-
825 dependent switching events dictate cell-lineage determination', *Cell*, 125: 593-605.
826 Perez-Castro, C., U. Renner, M. R. Haedo, G. K. Stalla, and E. Arzt. 2012. 'Cellular and molecular specificity of
827 pituitary gland physiology', *Physiol Rev*, 92: 1-38.
828 Plagge, A., E. Gordon, W. Dean, R. Boiani, S. Cinti, J. Peters, and G. Kelsey. 2004. 'The imprinted signaling
829 protein XL alpha s is required for postnatal adaptation to feeding', *Nat Genet*, 36: 818-26.
830 Potok, M. A., K. B. Cha, A. Hunt, M. L. Brinkmeier, M. Leitges, A. Kispert, and S. A. Camper. 2008. 'WNT
831 signaling affects gene expression in the ventral diencephalon and pituitary gland growth', *Dev Dyn*, 237:
832 1006-20.
833 Puertas-Avendano, R. A., M. J. Gonzalez-Gomez, M. D. Ruvira, M. J. Ruiz-Hidalgo, N. Morales-Delgado, J.
834 Laborda, C. Diaz, and A. R. Bello. 2011. 'Role of the non-canonical notch ligand delta-like protein 1 in
835 hormone-producing cells of the adult male mouse pituitary', *J Neuroendocrinol*, 23: 849-59.

836 Raghunandan, R., M. Ruiz-Hidalgo, Y. Jia, R. Ettinger, E. Rudikoff, P. Riggins, R. Farnsworth, A. Tesfaye, J.
837 Laborda, and S. R. Bauer. 2008. 'Dlk1 influences differentiation and function of B lymphocytes', *Stem*
838 *Cells Dev*, 17: 495-507.
839 Rizzoti, K., H. Akiyama, and R. Lovell-Badge. 2013. 'Mobilized adult pituitary stem cells contribute to endocrine
840 regeneration in response to physiological demand', *Cell Stem Cell*, 13: 419-32.
841 Russell, J. P., X. Lim, A. Santambrogio, V. Yianni, Y. Kemkem, B. Wang, M. Fish, S. Haston, A. Grabek, S.
842 Hallang, E. J. Lodge, A. L. Patist, A. Schedl, P. Mollard, R. Nusse, and C. L. Andoniadou. 2021.
843 'Pituitary stem cells produce paracrine WNT signals to control the expansion of their descendant
844 progenitor cells', *Elife*, 10.
845 Russell, J. P., E. J. Lodge, and C. L. Andoniadou. 2018. 'Basic Research Advances on Pituitary Stem Cell
846 Function and Regulation', *Neuroendocrinology*, 107: 196-203.
847 Satija, R., J. A. Farrell, D. Gennert, A. F. Schier, and A. Regev. 2015. 'Spatial reconstruction of single-cell gene
848 expression data', *Nat Biotechnol*, 33: 495-502.
849 Scagliotti, V., R. Costa Fernandes Esse, T. L. Willis, M. Howard, I. Carrus, E. Lodge, C. L. Andoniadou, and M.
850 Charalambous. 2021. 'Dynamic Expression of Imprinted Genes in the Developing and Postnatal
851 Pituitary Gland', *Genes (Basel)*, 12.
852 Schindelin, J., I. Arganda-Carreras, E. Frise, V. Kaynig, M. Longair, T. Pietzsch, S. Preibisch, C. Rueden, S.
853 Saalfeld, B. Schmid, J. Y. Tinevez, D. J. White, V. Hartenstein, K. Eliceiri, P. Tomancak, and A.
854 Cardona. 2012. 'Fiji: an open-source platform for biological-image analysis', *Nat Methods*, 9: 676-82.
855 Schmidt, J. V., P. G. Matteson, B. K. Jones, X. J. Guan, and S. M. Tilghman. 2000. 'The Dlk1 and Gtl2 genes are
856 linked and reciprocally imprinted', *Genes Dev*, 14: 1997-2002.
857 Skowronska-Krawczyk, D., Q. Ma, M. Schwartz, K. Scully, W. Li, Z. Liu, H. Taylor, J. Tollkuhn, K. A. Ohgi, D.
858 Notani, Y. Kohwi, T. Kohwi-Shigematsu, and M. G. Rosenfeld. 2014. 'Required enhancer-matrin-3
859 network interactions for a homeodomain transcription program', *Nature*, 514: 257-61.
860 Smas, C. M., L. Chen, and H. S. Sul. 1997. 'Cleavage of membrane-associated pref-1 generates a soluble
861 inhibitor of adipocyte differentiation', *Mol Cell Biol*, 17: 977-88.
862 Smas, C. M., and H. S. Sul. 1993. 'Pref-1, a protein containing EGF-like repeats, inhibits adipocyte
863 differentiation', *Cell*, 73: 725-34.
864 Stuart, T., A. Butler, P. Hoffman, C. Hafemeister, E. Papalexi, W. M. Mauck, 3rd, Y. Hao, M. Stoeckius, P.
865 Smibert, and R. Satija. 2019. 'Comprehensive Integration of Single-Cell Data', *Cell*, 177: 1888-902 e21.
866 Sul, H. S. 2009. 'Minireview: Pref-1: Role in Adipogenesis and Mesenchymal Cell Fate', *Molecular*
867 *Endocrinology*, 23: 1717-25.
868 Takada, S., M. Tevendale, J. Baker, P. Georgiades, E. Campbell, T. Freeman, M. H. Johnson, M. Paulsen, and
869 A. C. Ferguson-Smith. 2000. 'Delta-like and gtl2 are reciprocally expressed, differentially methylated
870 linked imprinted genes on mouse chromosome 12', *Curr Biol*, 10: 1135-8.
871 Taniguchi, Y., S. Yasutaka, R. Kominami, and H. Shinohara. 2001. 'Proliferation and differentiation of pituitary
872 somatotrophs and mammotrophs during late fetal and postnatal periods', *Anat Embryol (Berl)*, 204: 469-
873 75.
874 Tsai, C. E., S. P. Lin, M. Ito, N. Takagi, S. Takada, and A. C. Ferguson-Smith. 2002. 'Genomic imprinting
875 contributes to thyroid hormone metabolism in the mouse embryo', *Curr Biol*, 12: 1221-6.
876 Tucci, V., A. R. Isles, G. Kelsey, A. C. Ferguson-Smith, and Group Erice Imprinting. 2019. 'Genomic Imprinting
877 and Physiological Processes in Mammals', *Cell*, 176: 952-65.
878 Varrault, A., C. Gueydan, A. Delalbre, A. Bellmann, S. Houssami, C. Aknin, D. Severac, L. Chotard, M. Kahli, A.
879 Le Digarcher, P. Pavlidis, and L. Journot. 2006. 'Zac1 regulates an imprinted gene network critically
880 involved in the control of embryonic growth', *Dev Cell*, 11: 711-22.
881 Wang, Y., L. Zhao, C. Smas, and H. S. Sul. 2010. 'Pref-1 interacts with fibronectin to inhibit adipocyte
882 differentiation', *Mol Cell Biol*, 30: 3480-92.
883 Zhang, Z., M. Zamojski, G. R. Smith, T. L. Willis, V. Yianni, N. Mendelev, H. Pincas, N. Seenarine, M. A. S.
884 Amper, M. Vasoya, W. S. Cheng, E. Zaslavsky, V. D. Nair, J. L. Turgeon, D. J. Bernard, O. G.
885 Troyanskaya, C. L. Andoniadou, S. C. Sealfon, and F. Ruf-Zamojski. 2022. 'Single nucleus
886 transcriptome and chromatin accessibility of postmortem human pituitaries reveal diverse stem cell
887 regulatory mechanisms', *Cell Rep*, 38: 110467.
888 Zhu, X., J. Zhang, J. Tollkuhn, R. Ohsawa, E. H. Bresnick, F. Guillemot, R. Kageyama, and M. G. Rosenfeld.
889 2006. 'Sustained Notch signaling in progenitors is required for sequential emergence of distinct cell
890 lineages during organogenesis', *Genes Dev*, 20: 2739-53.